

A ~ 7.5 Earth-Mass Planet Orbiting the Nearby Star, GJ 876

Eugenio J. Rivera^{2,3,4}, Jack J. Lissauer³, R. Paul Butler⁴, Geoffrey W. Marcy⁵, Steven S. Vogt², Debra A. Fischer⁶, Timothy M. Brown⁷, Gregory Laughlin², Gregory W. Henry^{8,9}

rivera@ucolick.org

ABSTRACT

High precision, high cadence radial velocity monitoring over the past 8 years at the W. M. Keck Observatory reveals evidence for a third planet orbiting the nearby (4.69 pc) dM4 star GJ 876. The residuals of three-body Newtonian fits, which include GJ 876 and Jupiter mass companions b and c, show significant power at a periodicity of 1.9379 days. Self-consistently fitting the radial velocity data with a model that includes an additional body with this period significantly improves the quality of the fit. These four-body (three-planet) Newtonian fits find that the minimum mass of companion “d” is $m \sin i = 5.89 \pm 0.54 M_{\oplus}$ and that its orbital period is $1.93776 (\pm 7 \times 10^{-5})$ days. Assuming coplanar orbits, an inclination of the GJ 876 planetary system to the plane of the sky of $\sim 50^{\circ}$ gives the best fit. This inclination yields a mass for companion d of $m = 7.53 \pm 0.70 M_{\oplus}$, making it by far the lowest mass companion yet found around a main sequence star other than our Sun. Precise photometric observations at Fairborn

¹Based on observations obtained at the W.M. Keck Observatory, which is operated jointly by the University of California and the California Institute of Technology.

²UCO/Lick Observatory, University of California at Santa Cruz, Santa Cruz, CA 95064

³NASA/Ames Research Center, Space Science and Astrobiology Division, MS 245-3, Moffett Field, CA 94035

⁴Department of Terrestrial Magnetism, Carnegie Institution of Washington, 5241 Broad Branch Road NW, Washington DC, 20015-1305

⁵Department of Astronomy, University of California, Berkeley, CA 94720

⁶Department of Physics and Astronomy, San Francisco State University, San Francisco, CA 94132

⁷High Altitude Observatory, National Center for Atmospheric Research, P.O. Box 3000, Boulder, CO 80307

⁸Center of Excellence in Information Systems, Tennessee State University, 3500 John A. Merritt Blvd., Box 9501, Nashville, TN 37209

⁹Department of Physics and Astronomy, Vanderbilt University, Nashville, TN 37235

Observatory confirm low-level brightness variability in GJ 876 and provide the first explicit determination of the star’s 96.7-day rotation period. Even higher precision short-term photometric measurements obtained at Las Campanas imply that planet d does not transit GJ 876.

Subject headings: stars: GJ 876 – planetary systems – planets and satellites: general

1. Introduction

GJ 876 (HIP 113020) is the lowest mass star currently known to harbor planets. The first companion discovered, “b,” was announced by Marcy et al. (1998) and Delfosse et al. (1998). They found that this companion had an orbital period, P_b , of ~ 61 days and a minimum mass ($m_b \sin i_b$) of $\sim 2.1 M_{\text{Jup}}$ and that it produced a reflex barycentric velocity variation of its dM4 parent star of amplitude $K_b \sim 240 \text{ m s}^{-1}$. After 2.5 more years of continued Doppler monitoring, Marcy et al. (2001) announced the discovery of a second companion, “c.” This second companion has an orbital period, P_c , of ~ 30 days, $m_c \sin i_c \sim 0.56 M_{\text{Jup}}$, and $K_c \sim 81 \text{ m s}^{-1}$. As a result of fitting the radial velocity data with a model with two non-interacting companions, the fitted parameters for companion b were different, with the most significant change in K_b (and correspondingly $m_b \sin i_b$), which dropped from 240 m s^{-1} to 210 m s^{-1} .

Marcy et al. (2001) noted that although a model with two planets on unperturbed Keplerian orbits produces a very significantly improved fit to the radial velocity data by dramatically reducing both the $\sqrt{\chi_\nu^2}$ and the RMS of the fit¹⁰, these two statistics were still relatively large. A $\sqrt{\chi_\nu^2}$ of ~ 1.0 is expected for a model that is a “good” fit to the data assuming normally (Gaussian) distributed errors. Additionally, dynamical simulations based on this model showed that the system’s stability is strongly dependent on the starting epoch, which is used to determine the initial positions of the planets for the integrations. This indicated that the mutual perturbations among the planets are substantial on orbital timescales (Marcy et al. 2001). Laughlin & Chambers (2001) and Rivera & Lissauer (2001) independently developed self-consistent “Newtonian” fitting schemes which incorporate the

¹⁰The χ^2 is the sum of the squares of the differences between the data points and model points at each observed epoch divided by the corresponding uncertainties of the measurements. The reduced chi-squared, χ_ν^2 , is that quantity divided by the number of degrees of freedom (the total number of observations minus the number of fitted parameters). The RMS is the root-mean-square of the velocity residuals after the model fit has been subtracted from the data. Note that χ^2 has no units, and RMS has units of m s^{-1} in this case.

mutual perturbations among the planets in fitting the radial velocity data. Nauenberg (2002) developed a similar method which additionally gives a lower limit on the mass of the star; using the radial velocity data from Marcy et al. (2001), he found the mass of GJ 876 to be $M_\star > 0.3 M_\odot$. This dynamical modeling resulted in a substantially improved fit to the radial velocity data.

Laughlin et al. (2005) provide an updated analysis of the GJ 876 planetary system in which they perform 3-body (two-planet) fits to a radial velocity data set which includes 16 old observations taken at Lick observatory and observations taken at the Keck observatory up to the end of the 2003 observing season. In their fits, they have assumed a stellar jitter of 6 ms^{-1} . They found that the two jovian-mass planets are deeply in both the 2:1 mean motion resonance and in an apsidal resonance in which the longitudes of periastron remain nearly aligned. All three resonant angles librate with small amplitudes, which argues for a dissipative history of differential migration for the giant planets. Additionally, they were able to constrain the inclination of the coplanar system to the plane of the sky to be $i > 20^\circ$. Finally, they examined the possibility that if companion c is not transiting now, transits might occur in the future for non-coplanar configurations with modest mutual inclinations.

In this paper, we describe the results of a more detailed analysis using a new radial velocity data set. Note that most of the fits presented in this work do not take stellar jitter (which is found to be $\lesssim 1.5 \text{ ms}^{-1}$, see Section 5) into account. In Section 2, we present the new velocities and describe the procedures which resulted in significant improvements in the precision of these velocities. In Section 3, we incorporate the techniques from Laughlin et al. (2005) to determine the uncertainties in the parameters from two-planet fits. In Section 4, we present a periodogram analysis of the residuals to the two-planet fit, which suggests the presence of a third companion to GJ 876, with a period of 1.94 days. In Section 5, we present the results from three-planet fits, which provide estimates of the actual masses of companions b and c as well as $m_d \sin i_d$ of the small inner planet. The residuals of the 2-planet fit also show significant power at 2.0548 days; as discussed in Section 6, we have demonstrated that this second period is an alias of the 1.9379-day period. Section 7 presents the results of long-term photometric monitoring of GJ 876. In Section 8, we show that the third companion was not transiting in 2003. We discuss some interesting aspects of the third companion in Section 9. Finally, we end with a summary of our results and our conclusions.

2. Radial Velocity Observations

The stellar characteristics of GJ 876 (M4 V) have been described previously in Marcy et al. (1998) and Laughlin et al. (2005). It has a Hipparcos distance of 4.69 pc (Perryman

et al. 1997). From its distance and the bolometric correction of Delfosse et al. (1998), its luminosity is $0.0124 L_{\odot}$. As in previous studies, we adopt a stellar mass of $0.32 M_{\odot}$ and a radius of $0.3 R_{\odot}$ based on the mass-luminosity relationship of Henry & McCarthy (1993). We do not incorporate uncertainties in the star’s mass ($0.32 \pm 0.03 M_{\odot}$) into the uncertainties in planetary masses and semi-major axes quoted herein. The age of the star is roughly in the range 1–10 Gyr (Marcy et al. 1998).

We searched for Doppler variability using repeated, high resolution spectra with resolving power $R \approx 70000$, obtained with the Keck/HIRES spectrometer (Vogt et al. 1994). The Keck spectra span the wavelength range from 3900–6200 Å. An iodine absorption cell provides wavelength calibration and the instrumental profile from 5000 to 6000 Å (Marcy & Butler 1992, Butler et al. 1996). Typical signal-to-noise ratios are 100 per pixel for GJ 876. At Keck we routinely obtain Doppler precision of $3-5 \text{ m s}^{-1}$ for $V = 10$ M dwarfs, as shown in Figure 1. A different set of 4 stable Keck M dwarfs is shown in Figure 2 of Butler et al. (2004). The variations in the observed radial velocities of these stars can be explained by the internal uncertainties in the individual data points; thus, there is no evidence that any of these stars possess planetary companions. Exposure times for GJ 876 and other $V = 10$ M dwarfs are typically 8 minutes.

The internal uncertainties in the velocities are judged from the velocity agreement among the approximately 400 2-Å chunks of the echelle spectrum, each chunk yielding an independent Doppler shift. The internal velocity uncertainty of a given measurement is the uncertainty in the mean of the ~ 400 velocities from one echelle spectrum.

We present results of N-body fits to the radial velocity data taken at the W. M. Keck telescope from June 1997 to December 2004. The 155 measured radial velocities are listed in Table 1. The median of the uncertainties is 4.1 m s^{-1} . Comparison of these velocities with those presented in Laughlin et al. (2005) shows significant changes (typically $3-10 \text{ m s}^{-1}$) in the velocities at several observing epochs.

The changes in the measured velocities are a result of a more sophisticated modeling of the spectrum at sub-pixel levels and of key improvements in various instrumental idiosyncrasies. The previous HIRES CCD, installed at first-light in 1993, had 1) relatively large ($24 \mu\text{m}$) pixels, 2) a convex surface, 3) excessive charge diffusion in the CCD substrate, which broadened the detector’s point spread function (PSF), and 4) a subtle signal-dependent non-linearity in charge transfer efficiency (CTE). These combined effects had been limiting our radial velocity precision with HIRES to about 3 m s^{-1} since 1996. In August 2004, the old CCD was replaced by a new 3-chip mosaic of MIT-Lincoln Labs CCDs. These devices provided a very flat focal plane (improving the optical PSF), a finer pixel pitch (which improved our sub-pixel modeling), and more spectral coverage per exposure. The MIT-LL devices also

are free of signal-dependent CTE non-linearities and have a much lower degree of charge diffusion in the CCD substrate (which improved the detector PSF). We also switched into higher cadence mode in October, 2004, observing 3 times per night and for as many consecutive nights as telescope scheduling would allow. Additionally, toward the end of 2004, a high signal-to-noise template of GJ 876 was obtained. All Keck data were then re-reduced using the improved Doppler code together with the new high S/N template and the higher cadence 2004 observations. As a result of the improvements, the two- (and three-) planet fits presented here for this system are significantly improved over previous N-body fits.

3. Two-Planet Coplanar Fits

We first performed self-consistent 2-planet fits in which we assumed that the orbits of both companions “b” and “c” are coplanar and that this plane contains the line of sight ($i_b = i_c = 90^\circ$). These are fits to all the 155 Keck radial velocities listed in Table 1. All fits were obtained with a Levenberg-Marquardt minimization algorithm (Press et al. 1992) driving an N-body integrator. This algorithm is a more general form of the algorithms used in Laughlin & Chambers (2001) and Rivera & Lissauer (2001). All fits in this work are for epoch JD 2452490, a time near the center of the 155 radial velocity measurements. We fitted for 10+1 parameters; 10 of these parameters are related to the planetary masses and orbital elements: the planetary masses (m), the semi-major axes (a), eccentricities (e), arguments of periastron (ω), and mean anomalies (M) of each body, and 1 parameter is for the radial velocity offset, representing the center-of-mass motion of the GJ 876 system relative to the barycenter of our Solar System and arbitrary zero-point of the velocities.

We first obtained a nominal 2-planet fit to the actual 155 observed velocities. Figure 2 shows the model radial velocity (solid line) generated from this nominal 2-planet fit, along with the actual observed velocities (solid points with vertical error bars); the residuals are shown in the lower portion. Table 2 shows the best fitted parameters, which are similar to those obtained by Laughlin et al. (2005). The osculating orbital elements (for epoch JD 2452490) listed in Table 2 are in Jacobi coordinates. In these coordinates, each planet is explicitly assumed to be in orbit about the center of mass of all bodies interior to its orbit. As explained in Lissauer & Rivera (2001) and Lee & Peale (2003), Jacobi coordinates are the most natural system for expressing multiple-planet fits to radial velocity data.

The uncertainties listed in Table 2 were obtained by performing 1000 additional 2-planet fits to 1000 radial velocity data sets generated using the bootstrap technique described in Section 15.6 of Press et al. (1992). Each velocity data set consisted of 155 entries chosen at random from the 155 entries in the actual velocity data set (Table 1). Each entry consists

of the observing epoch, the velocity measurement, and the instrumental uncertainty. For every choice, all 155 entries were available to be chosen. This procedure results in generated velocity data sets that contain duplicate entries. The fitting algorithm cannot handle such a data set. Thus, when an entry is chosen more than once during the generation of a velocity data set, 0.001 day is added to the observing epoch of each duplicate entry. We then performed 2-planet fits to each of these 1000 velocity data sets, using the parameters from the nominal 2-planet fit in the initial guesses. The 1000 fits result in ranges in the fitted values of each of the parameters. The uncertainties listed in Table 2 are the standard deviations of the distributions of the parameters.

Using an earlier data set of radial velocity measurements, we had also performed an analysis to determine uncertainties in the fitted parameters like the one above and an analysis using randomized residuals (described in Section 6) in which a model is assumed to generate synthetic data sets. There was no (significant) difference in the resulting uncertainties. For the data set used in this work, we use just the bootstrap method to determine the uncertainties in the fitted parameters since this technique is not constrained by an assumed model. It should be noted that it is not a problem to apply the bootstrap method in determining the uncertainties in the parameters since the method in which the parameters are determined (χ^2 minimization) does not depend on the order in which (the square of) the differences between the model and observed velocities are summed. That is, the data points are identically distributed (see pp. 686 and 687 in Press et al. 1992).

The uncertainties determined using the bootstrap method explicitly *do not* account for the correlations which exist among the fitted orbital parameters. On the other hand, the uncertainties determined from the Levenberg-Marquardt routine *do* account for the correlations. An example involving e and ω illustrates the differences. In general, from the Levenberg-Marquardt routine, a small fitted value for e results in a large uncertainty in ω , and a large value for e results in a small uncertainty in ω . Thus, if the uncertainty in e is large, the uncertainty in ω may be misleading since it depends on the fitted value of e (whereas the actual value of e could be any value within the range of its uncertainty). The bootstrap method is able to explore the full range of possible values of both e and ω simultaneously.

It is possible that the bootstrap method can give different uncertainties if we use different initial guesses. However, for the GJ 876 system with an assumed coplanar configuration, we have verified that the fitted parameters are relatively robust to changes in the initial guesses (Rivera & Lissauer 2001). When we explore systems with mutual inclinations, multiple minima appear (see Section 5). Thus, varying the initial guesses while using the bootstrap method to determine uncertainties becomes more relevant for fits with mutual inclinations.

In agreement with previous studies, we find that the system corresponding to the parameters in Table 2 is also deeply in the 2:1 mean motion resonance and in the apsidal resonance. We performed 1000 simulations (for 10 years each) based on the nominal fit in Table 2 and the 1000 fits used to determine the uncertainties in the parameters. The three critical arguments, $\theta_1 = \lambda_c - 2\lambda_b + \varpi_c$, $\theta_2 = \lambda_c - 2\lambda_b + \varpi_b$, and $\theta_3 = \varpi_c - \varpi_b$, where λ_c and λ_b are the respective mean longitudes of companions c and b and ϖ_c and ϖ_b are the corresponding longitudes of periastron, all librate about 0° with the following small amplitudes: $|\theta_1|_{max} = 5.6 \pm 1.4^\circ$, $|\theta_2|_{max} = 28.8 \pm 8.4^\circ$, and $|\theta_3|_{max} = 29.0 \pm 9.3^\circ$. These amplitudes are smaller than but consistent with the values from Laughlin et al. (2005). Note that all three critical arguments have approximately the same period of libration (~ 8.8 yr).

The overall long-period (~ 8.8 yr) envelope of the model radial velocity in Figure 2 arises from beating between the periods of the jovian-mass planets, since the periods are not exactly commensurate. The radial velocity reversals occur when planets b and c are on opposite sides of the star, which occurs roughly every 60 days. An inspection of the two components of the radial velocity due to companions b and c, the sum of these two velocities, and the mean anomalies of planets b and c shows that the reversals occur when c is near periastron ($M_c \sim 0^\circ$) while b is near apastron ($M_b \sim 180^\circ$). Thus, reversals occur when the (full) orbital velocity of companion b is near a minimum while that of c is near a maximum. This configuration arises because of the resonant state of the system. Also, the acceleration of the star due to companion c when it is at periastron, $Gm_c/(a_c(1 - e_c))^2 = 0.0339 \text{ cm s}^{-2}$ (simply using the values from Table 2), is greater than that due to companion b when it is at apastron, $Gm_b/(a_b(1 + e_b))^2 = 0.0239 \text{ cm s}^{-2}$. In comparison, the mean acceleration of the star due to planet c is $Gm_c/a_c^2 = 0.0205 \text{ cm s}^{-2}$, and that due to planet b is $Gm_b/a_b^2 = 0.0252 \text{ cm s}^{-2}$. Inspection of the longitudes of periastron for planets b and c also shows that the vertical position in Figure 2 and amplitude of a velocity reversal is correlated with the longitude of periastron (of both companions). The largest velocity reversals occur when the lines of apsides are roughly perpendicular to the line of sight ($\omega \sim 0$ or 180°), and these occur near maxima in the full radial velocity of the star (e.g., near epochs JD 2451060, where $\omega \sim 360^\circ$, and JD 2452600, where $\omega \sim 180^\circ$, in Figure 2). The period of this vertical traversal of the reversals coincides with the period of circulation of the periastron longitudes (~ 8.8 yr). Note that in a two-Keplerian model, reversals are also present, and they appear to move vertically (Marcy et al. 2001). However, in the two-Keplerian case, the vertical displacement results from the periods not being exactly commensurate. In this case the line joining the planets when they are on opposite side of the star will deviate farther and farther from the line of apsides. As a result, the shapes of the reversals in the two types of models appear different (Laughlin et al. 2005).

As in previous studies, we considered various inclinations of the coplanar system and

generated a series of 2-planet (10+1 parameter) fits. Figure 3 shows the resulting $\sqrt{\chi_\nu^2}$ for the 2-planet fits versus the inclination (i) as triangles. Note that $\sqrt{\chi_\nu^2}$ starts to rise when $i \lesssim 50^\circ$. Laughlin et al. (2005) found that $\sqrt{\chi_\nu^2}$ starts to rise only when $i \lesssim 40^\circ$. The stricter constraint that we are able to derive is primarily a result of the improvements to the measurements mentioned in Section 2. Moreover, although previous studies (Laughlin & Chambers 2001; Rivera & Lissauer 2001; Laughlin et al. 2005) only found a very shallow minimum in $\sqrt{\chi_\nu^2}$ versus i , the minimum for our larger, more precise data set is noticeably deeper. Newtonian models yield far better fits to the data than do Keplerian models because there is a clear signal of periape regression in the data (Ford 2005). However, this observed regression rate can be matched by models with relatively low mass planets b and c (high $\sin i$) on low eccentricity orbits, or higher mass planets on more eccentric orbits. The $\sqrt{\chi_\nu^2}$ increases only when planetary eccentricities (and masses) become too large, and the shape of the model velocity curve starts to deviate significantly from the data. Note that a large value of $\sqrt{\chi_\nu^2}$ for a given small value of i does not immediately imply that a system with such a value for i is unstable on short timescales (< 10 Myr). Indeed, Rivera & Lissauer (2001) found that a system with $i \sim 11.5^\circ$ was stable for at least 500 Myr.

4. Residuals to the Two-Planet Fit

We performed a (Lomb) periodogram analysis (Section 13.8 in Press et al. 1992) to the residuals of the 2-planet $i = 90^\circ$ fit. The result is displayed in Figure 4 and shows a maximum peak (the peak with the largest power) with very significant power, i.e., much higher than typical variations, at a period of 1.9379 days. The periodograms of the residuals of all of the 2-planet coplanar fits in which we varied the inclination of the system show a maximum peak at ~ 1.94 days. This periodicity is also present as the largest peak in 995 periodograms of the 1000 residuals of the 2-planet coplanar fits used to determine the uncertainties in Table 2. We performed 2-planet $i = 90^\circ$ fits to various subsets of the first or last N data points, and the periodicity is also present as the largest peak in the periodograms of all of the corresponding residuals; the amount of power at 1.94 days rises with N . Additionally, the blue points in Figure 5 directly show the phased residuals of the two-planet fit, folded with a period of 1.9379 days. The red points in Figure 5 show the phased residuals of the 2-planet, $i = 50^\circ$ coplanar fit. We carried out a double-Keplerian fit to subsets of the radial velocities, each of which contained the data for one observing season with a high cadence of observations, and computed the periodogram of the residuals. The sum of all such periodograms exhibited its tallest peak at a period of 1.94 d, in agreement with the best period found from our dynamical models. This test shows that the 1.94 d period cannot be an artifact of the dynamical modeling but rather is inherent in the data.

These results provide evidence that GJ 876 likely has a third companion, “d.” The second, smaller peak in Figure 4, at 2.0548 days with power ~ 26 , is likely an alias, and this issue is addressed in Section 6. The ratio of the power in the two periods is 1.3394. In the following two sections, we refer to these two periodicities by their approximate values of 1.94 and 2.05 days, respectively.

An alternative to the third planet hypothesis is that this periodicity is due to pulsation of the star itself. For the dM2.5 dwarf GJ 436, Butler et al. (2004) reported a planet having $m \sin i = 21 M_{\oplus}$ with $P = 2.8$ days and $K = 18 \text{ m s}^{-1}$. Otherwise, none of the 150 M0-M5 dwarfs on the Keck planet search survey exhibits any periodicity with a 2-day period. This suggests that M dwarfs do not naturally pulsate at such a period. Moreover, we are not aware of any timescale within M dwarfs corresponding to 2 days. The dynamical and acoustical timescale, analogous to the Solar 5-minute oscillations, would similarly be of order minutes for M dwarfs. We therefore rule out acoustic modes as the cause of the 2-day period. The rotation period of GJ 876 is at least ~ 40 days, based on its narrow spectral lines and its low chromospheric emission at Ca II H&K (Delfosse et al. 1998); we present photometric evidence of a rotation period of 97 days in Section 7. Thus, rotational modulation of surface features cannot explain the 2-day period in the velocities. Similarly, gravity modes and magnetic buoyant processes seem unlikely to explain the high-Q periodicity that we detect over the timespan of 8 years in GJ 876. Thus, the 2-day periodicity in velocity cannot be easily explained by any known property of this normal M dwarf.

5. Three-Planet Fits

Based on the results of the periodogram analysis presented in the previous section, we performed 3-planet self-consistent fits with the period of the third planet initially guessed to be about 1.94 days. These 3-planet fits involve 13+1 parameters; the 3 new fitted parameters are the mass, semi-major axis, and mean anomaly of the third planet, and the remaining 10+1 parameters are the same as in the 2-planet fits described in Section 3. Because of the strong eccentricity damping effects of tides at its distance from the star, the third planet was assumed to be on a circular orbit. Note that this assumption is relaxed later on for some fits.

As in Section 3, we performed a nominal 3-planet fit to obtain the best fitted parameters plus 1000 additional 3-planet fits to obtain the uncertainties in the parameters. For the nominal fits $\sqrt{\chi_{\nu}^2} = 1.154$ and $\text{RMS}=4.59 \text{ m s}^{-1}$ for 3 planets, compared to $\sqrt{\chi_{\nu}^2} = 1.593$ and $\text{RMS}=6.30 \text{ m s}^{-1}$ for 2 planets. Like Table 2 in Section 3, Table 3 shows the best fitted parameters for the 3-planet fit with $i = 90^{\circ}$.

Figure 6 shows the phased velocity contributions due to each planet. This figure is analogous to Figure 10 in Marcy et al. (2002), which shows the triple-*Keplerian* orbital fit to the radial velocities for 55 Cancri. The major difference is that our Figure 6 shows a triple-*Newtonian* fit. Both the data and the model show the interactions between GJ 876’s planets. However, in generating Figure 6 all of the data are folded into the first orbital period after the first observing epoch, while the models only show the velocities during that first period (in all three panels, the velocities shown in the second period are duplicated from the first period). Since the osculating orbital elements for the outer two planets are varying due to mutual perturbations, the data should deviate from the model, as clearly shown for companions b and c. Since companion d is largely decoupled from the outer planets (in both the data and the model), the observed velocities more closely match the model, and the deviations shown are primarily due to the residual velocities. The decoupling is a consequence of the large ratio of the orbital periods for planets c and d (> 15).

The parameters for the two previously known outer planets are not significantly affected by fitting for the parameters for all three planets. However, all of the uncertainties of these parameters are reduced. Thus, the addition of the third planet does not have as significant an effect on the planetary parameters as the effect that the addition of companion c had on changing the parameters of companion b. This result isn’t surprising, given the very low mass and very different orbital period of planet d.

These results have led us to the likely interpretation of a third companion to GJ 876 with a minimum mass of $m_d \sin i_d \sim 6 M_\oplus$ and a period of about 2 days. Although this planet is the lowest mass extrasolar planet yet discovered around a main sequence star, even lower mass planets have been found around the millisecond pulsar PSR B1247+1221 (Wolszczan & Frail 1992; Konacki & Wolszczan 2003).

We also generated a series of 3-planet (13+1 parameter) fits in which we varied the inclination of the coplanar system. Figure 3 shows $\sqrt{\chi_\nu^2}$ for the 3-planet fits versus the inclination as squares. The global minimum in $\sqrt{\chi_\nu^2}$ (1.061 with an RMS of 4.23 m s^{-1}) occurs at $i = 50^\circ$, almost precisely the location of the minimum for the two-planet fits. As for the two-planet fits, the $\sqrt{\chi_\nu^2}$ starts to rise when $i < 50^\circ$. Unlike two-planet fits performed on previous data sets, the minimum at $i = 50^\circ$ is significant. Using the bootstrap method as in Press et al. (1992), we generated 100 velocity data sets and performed a series of 71 fits ($i = 90^\circ, i = 89^\circ, \dots, i = 20^\circ$) to each set in which we varied the inclination of the system. This results in 100 curves which are analogous to the lower curve in Figure 3. Ninety-eight of these curves have a minimum in $\sqrt{\chi_\nu^2}$ which occurs at $i = 45\text{--}58^\circ$. Seventy-nine have a minimum at $i = 48\text{--}52^\circ$. Considering all 100 curves, the mean value (and standard deviation) of the location of the minimum in $\sqrt{\chi_\nu^2}$ is $i = 50.2 \pm 3.1^\circ$, and the median value

is 50° . The mean value (and standard deviation) of the drop in $\sqrt{\chi_\nu^2}$ from the value at $i = 90^\circ$ to the value at the minimum is 0.094 ± 0.036 , and the median is 0.097. The mean value (and standard deviation) of the drop in $\sqrt{\chi_\nu^2}$ from the value at $i = 90^\circ$ to the value at $i = 50^\circ$ is 0.091 ± 0.036 , and the median is 0.095. These values are fully consistent with the drop observed for the actual data. Figure 7 shows the entire set of results (small points) along with the results from fitting the real data (squares). Figure 8 shows the model radial velocity generated from the $i = 50^\circ$ 3-planet fit to the actual data, along with the actual observed velocities; the residuals are shown in the lower portion. Note that the residuals in Figure 8 are shown on the same scale as in Figure 2; the dispersion is clearly smaller in the 3-planet fit. For completeness, Figure 9 overlays the two model curves from Figures 2 and 8 and the data near the epoch JD 2452060; this illustrates the effect that the third planet has on the model. Table 4 lists the best fitted orbital parameters for $i = 50^\circ$. As in Tables 2 and 3, the uncertainties listed in Table 4 are based on 1000 fits with $i = 50^\circ$. The top panel of Figure 10 shows the periodogram of the residuals for this fit. There are no clearly significantly strong peaks (but see Section 9).

We analyzed the significance of the minimum at $i = 50^\circ$ by performing a limited set of fits in which the orbits of planets b and c have a mutual inclination. An exhaustive search of the entire 20+1 parameter space delimited by the masses and six orbital parameters of each of the three planets, less one representing rotation of the entire system about the line of sight, is beyond the scope of this paper. One complication arises from the appearance of a significant number of multiple minima. For example, Rivera & Lissauer (2001) found several satisfactory two-planet fits (with similar values of $\sqrt{\chi_\nu^2}$) which had significantly different fitted orbital parameters. We did, however, fit parameters for two sets of non-coplanar planetary configurations. In both cases, the planetary orbital planes at epoch were fixed such that the tiny inner planet and one of the giant planets were coplanar with orbit normal inclined at epoch by 50° from the line of sight, and the other giant planet’s orbit normal was inclined by a pre-determined amount from the line of sight with the same node as that of the other two planets, so that the mutual inclination was equal to the difference in inclination to the line of sight. Other initial parameters for the fitting were taken from the fit given in Table 4, with $m \sin i$, rather than m , conserved for the non-coplanar planet. In one set, the inner and middle planets had $i = 50^\circ$ and the outer planet’s inclination varied. In the other set of fits, the inner and outer planets had $i = 50^\circ$ and the middle planet’s inclination differed. The $\sqrt{\chi_\nu^2}$ of these fits are shown in Figure 11. Since only a small amount of the parameter space was explored, these preliminary results are only sufficient to draw two tentative conclusions: 1) since $\sqrt{\chi_\nu^2}$ rises more rapidly as the inclination of b is varied, the minimum in $\sqrt{\chi_\nu^2}$ appears primarily to constrain the inclination of companion b, and 2) the mutual inclination between the outer two planets is likely small. Note that since the

nodes were all the same in these fits, varying the mutual inclination changes the mass ratio of the planets; in contrast, varying the nodes can produce configurations with large mutual inclinations but similar mass ratios to those estimated assuming coplanar systems.

As for the two-planet case, the jovian-mass planets are deeply locked in the resonant state in three-planet simulations. For $i = 90^\circ$, $|\theta_1|_{max} = 5.9 \pm 1.1^\circ$, $|\theta_2|_{max} = 30.2 \pm 6.1^\circ$, and $|\theta_3|_{max} = 30.1 \pm 6.6^\circ$. Note that for the 3-planet simulations, the uncertainties of the amplitudes of the critical angles are reduced, as are the uncertainties in the parameters in Table 3. For $i = 50^\circ$, $|\theta_1|_{max} = 5.4 \pm 0.9^\circ$, $|\theta_2|_{max} = 19.5 \pm 3.8^\circ$, and $|\theta_3|_{max} = 19.4 \pm 4.3^\circ$. As in Laughlin et al. (2005), we find a general trend in which the amplitudes of the critical arguments decrease as i decreases.

We attempted to determine a dynamical upper limit to the mass of planet d. For a coplanar system with $i = 50^\circ$, the fitted m_d is $7.53 M_\oplus$. However, we find that the introduction of an inclination of planet d’s orbit to the initial orbital plane of planets b and c has little effect on $\sqrt{\chi_\nu^2}$. We performed a set of 3-planet fits in which we kept the outer two planets in the same plane with $i = 50^\circ$, but varied the inclination of companion d through values $< 50^\circ$. All three nodes were kept aligned. We find that $\sqrt{\chi_\nu^2}$ does not deviate significantly above 1.061 until $i_d < 3^\circ$. We then used the Mercury integration package (Chambers 1999), modified as in Lissauer & Rivera (2001) to simulate the general relativistic precession of the periastra, to perform simulations up to 1 Myr based on these fits, and find that the system is stable for $i_d \geq 3^\circ$. The fitted mass for planet d for the most inclined stable system is $\sim 103 M_\oplus$. This result indicates that the orbit normal of planet d may lie at least as close as 3° to the line of sight. The orbit normal could point toward or away from us. This defines a double cone which occupies a solid angle of 0.0172 steradians, or about 0.137% of 4π steradians. Even by restricting the parameter space by fixing $i_b = i_c = 50^\circ$, stability considerations can only exclude configurations with the orbit normal of companion d in this small solid angle. Thus, these stability considerations cannot presently provide a very meaningful upper bound on the mass of companion d.

With only $m \sin i$ determined here for the new planet, its actual mass and the value of i remain essentially unconstrained by dynamical considerations. Nearly pole-on orientations of the orbital plane cannot be ruled out. However, for randomly oriented orbital planes, the probability that the inclination is i or lower (more face-on) is given by $P(i) = 1 - \cos i$. Thus, for example, the probability that $\sin i < 0.5$ is 13%. Hence, it is *a priori* unlikely that $m_d > 2m_d \sin i_d$. Moreover, GJ 876 is the only M dwarf for which such intense Doppler observations have been made (due to the interest in the outer two planets). The population of M dwarfs from which this low $m \sin i$ was found is only one, namely GJ 876 itself. In contrast, more than 150 M stars have been observed with adequate precision to detect planets of Saturn

mass or greater in two day orbits, and most of these have been observed with adequate precision to detect a Neptune mass planet so close in. Yet apart from GJ 876, the only M star known to possess a planet is GJ 436, which has a companion with $m \sin i = 21 M_{\oplus}$ on a 2.644-day orbit (Butler et al. 2004). Therefore, the low $m \sin i$ of GJ 876 d was likely not drawn from some large reservoir for which a few nearly pole-on orbits might be expected. We conclude that the true mass of the new planet is likely to be $\lesssim 10 M_{\oplus}$.

We also performed analyses to place limits on the eccentricity of planet d. Two series of one-planet fits to the velocity residuals of both the $i = 90^\circ$ and $i = 50^\circ$ two-planet fits (Figure 5) suggest that the eccentricity of the third companion could be as high as ~ 0.22 . For the initial guesses, we used the best-fitted mass, period, and mean anomaly for companion d from the three-planet self-consistent fit (from Table 3 for $i = 90^\circ$ and from Table 4 for $i = 50^\circ$), but varied the initial guessed eccentricity and argument of periastron, and fitted for the eccentricity, argument of periastron, and mean anomaly. Figure 12 shows the resulting phased velocities for $i = 90^\circ$. Additionally, for both $i = 90^\circ$ and $i = 50^\circ$ we performed a few fits including all three planets and using an initial guessed eccentricity for the third planet $e_d \sim 0.22$. The largest fitted value is ~ 0.28 (for each value of i); this represents our best estimate for an upper limit on the eccentricity of companion d. Based on each of the best fit parameters in Tables 3 and 4, dynamical integrations of the system with the inner planet initially on a circular orbit show that the forced eccentricity of companion d is only ~ 0.0018 for $i = 90^\circ$ and ~ 0.0036 for $i = 50^\circ$. The tidal circularization timescale for a planet of mass m_{pl} and radius R_{pl} in an orbit with semi-major axis a about a star of mass M_* is

$$\tau = \frac{4}{63} Q \left(\frac{a^3}{GM_*} \right)^{1/2} \left(\frac{m_{\text{pl}}}{M_*} \right) \left(\frac{a}{R_{\text{pl}}} \right)^5 \quad (1)$$

(Goldreich & Soter 1966, Rasio et al. 1996). For GJ 876 d, for $i = 90^\circ$, $a = 0.021$ AU, $m_{\text{pl}} = 5.9 M_{\oplus}$ and $R_{\text{pl}} = 1.619 R_{\oplus}$ (see Section 8) this timescale is $< 10^5$ yr if companion d has a dissipation factor, Q , similar to that of Earth (~ 10). If the Q of companion d is similar to the estimated Q values for the outer planets in the Solar System ($10^4 - 10^5$), then the timescale for eccentricity damping would be 40–400 Myr, which is less than the estimated 1-10 Gyr lifetime of the star (Marcy et al. 1998). These arguments and results indicate that the eccentricity of companion d is fully consistent with 0.

We addressed the issue of stellar jitter by performing a few 3-planet, $i = 50^\circ$, fits in which we folded an assumed value of stellar jitter in quadrature into the instrumental uncertainties (listed in Table 1). The most relevant quantity in these fits is the $\sqrt{\chi^2_{\nu}}$. Although we only fit for 13+1 parameters at a time, by varying the inclination of the system, we effectively allowed a 15th free parameter. To account for this extra parameter, the formal $\sqrt{\chi^2_{\nu}}$ must be adjusted upwards by a factor of $\sqrt{141/140} \approx 1.0036$. (Note that the 141 and 140 are

the number of observations, 155, minus the number of fitted parameters, 13+1 and 14+1, respectively.) Accounting for this factor, and folding in an assumed jitter of 0, 0.5, 1.0, 1.5, and 2.0 m s^{-1} , the $\sqrt{\chi_\nu^2}$ are 1.065, 1.057, 1.034, 0.9996, and 0.956 respectively. These results indicate that the actual stellar jitter of GJ 876 is likely to be small ($\lesssim 1.5 \text{ m s}^{-1}$), as it is unlikely for the $\sqrt{\chi_\nu^2}$ to be substantially less than unity for a data set as large as the one used in this paper. Note that the period of companion d is the same to better than 1 part in 10^5 for all five values of the assumed stellar jitter.

6. Aliasing: What Is the Period of the Third Companion?

The periodogram presented in Section 4 shows significant power at both 1.94 days and 2.05 days. Using ~ 2.05 days as an initial guess for the period of the third planet, we performed a 3-planet fit to the observed radial velocities. The resulting fitted period for the third planet is 2.0546 days. More importantly, this fit is not vastly worse than the fit with the period of the third planet initially guessed to be 1.94 days ($\sqrt{\chi_\nu^2} = 1.154$ and $\text{RMS} = 4.59 \text{ m s}^{-1}$ for 1.94 days, and $\sqrt{\chi_\nu^2} = 1.290$ and $\text{RMS} = 5.08 \text{ m s}^{-1}$ for 2.05 days, compared with $\sqrt{\chi_\nu^2} = 1.593$ and $\text{RMS} = 6.30 \text{ m s}^{-1}$ for the corresponding 2-planet model). This result prompted a series of tests which together strongly support the hypothesis that the 1.94-day period is the correct one (and the 2.05-day period is an alias), as follows.

We first examined the periodograms of the residuals of the three-planet fits for each period (the lower two panels of Figure 10), and we detected no peaks with very significant power at any period (there is moderate power near 9 days and at other periods — see Section 9). The detection of a significant peak at 1.94 days in the residuals of the three-planet fit with $P_d = 2.05$ days would have been a clear indication that the 1.94-day period is the true period, because the introduction of a third planet with the wrong period should not (fully) account for the true periodicity. This simple test thus implies that one of the near two-day periods is an alias, but it does not indicate which period is the alias.

We then analyzed various mock velocity data sets to determine whether or not both near 2-day periodicities could result purely from the spacing of the observations and to determine the relative robustness of the two short-period planet solutions. We generated the mock velocity data sets for this study by randomizing residuals, as follows: The difference between the observed and modeled velocities results in a residual velocity at each observing epoch. We indexed the 155 residuals. At each observing epoch, we chose a random integer from 1 to 155 inclusive, and added the corresponding residual to the model velocity at that epoch.

One issue to address is whether the third periodicity (for both periods) is an artifact of

the observing frequency. We generated 1000 mock velocities by randomizing the residuals of the two-planet model and performed two-planet fits to these velocities. If the third periodicity is purely due to the observing frequency, then the periodograms of the residuals to these two-planet fits should show significant power at the third periodicity. Figure 13 shows the maximum power at the two periods in each of the 1000 periodograms. In not one case out of 1000 did we observe a periodogram which resembled the periodogram presented in Figure 4. Not one peak was found at either period that was as significant as the ones in the periodogram in Figure 4. In fact, for the 1.94-day period, the mean (and standard deviation) of the maximum power for the 1000 periodograms is 3.2 ± 1.4 . For the 2.05-day period, this is 3.1 ± 1.3 . The most significant peaks at either periodicity had a power of ~ 10 , about 38% of the power in the second highest peak in Figure 4. In Figure 4, the observed maximum peak at 1.94 days (~ 35) is > 22 standard deviations above the mean value of the maximum peaks determined in Figure 13. At 2.05 days, the observed power (~ 26) is > 17 standard deviations above the mean value of the maximum peaks determined in Figure 13. This strongly indicates that (at least) one of the periodicities must be real.

We performed similar experiments in which we generated 4000 sets of mock velocities based on the three-planet model. Using randomizing residuals, two thousand of the sets were generated based on the model in which the third planet had a period of 1.94 days. The remaining 2000 sets were generated in an analogous manner but based upon the model in which the third planet had a period of 2.05 days. We then performed two-planet fits to all 4000 velocity sets. Then, we examined the periodograms of the residuals of these fits to see if we could generate results similar to the one in Section 4. Figure 14 shows histograms of the ratio of the power at 1.94 days to the power at 2.05 days. Red is for the models with the third planet at 1.94 days, and blue is for the models with the third planet at 2.05 days. With a model in which the third planet had a period of 1.94 days, 1996 periodograms have a maximum peak at 1.94 days, and 278 have a ratio in the power at 1.94 days to the power at 2.05 days exceeding 1.3394 (478 have this ratio exceeding 1.3). Thus, the model with $P_d = 1.94$ days can yield periodograms which resemble the result when a two-planet fit is performed on the actual data. With a model in which the third planet had a period of 2.05 days, 79 periodograms have a maximum peak at 1.94 days, and 0 have a ratio in the power at 1.94 days to the power at 2.05 days exceeding 1.3394. Thus, the model with $P_d = 2.05$ days *never* resulted in a periodogram which resembles the result when a two-planet fit is performed on the actual data. This is very strong evidence that the 1.94-day period is the true period of the third companion.

Additional results also indicate that the 1.94-day period is the “better” one. Briefly, the $\sqrt{\chi^2}$ and RMS are smaller, and there is more power at 1.94 days in the periodogram of the residuals of the two-planet fit. For the three-planet fits, the osculating radial velocity

amplitude of the star, K , due to the third planet is $\sim 40\%$ larger than the RMS of the fit with $P_d = 1.94$ days, while this K is only 5% larger than the RMS for the fit with $P_d = 2.05$ days.

7. Photometric Variability in GJ 876

Very little is known about the photometric variability of GJ 876 on rotational and magnetic cycle timescales. Weis (1994) acquired 38 Johnson V and Kron RI measurements at Kitt Peak National Observatory over an 11 year period. He observed variability of a couple percent or so and suspected a possible periodicity of 2.9 years. Based on these findings, Kazarovets & Samus (1997) assigned GJ 876 the variable star name IL Aqr in *The 73rd Name List of Variable Stars*. The Hipparcos satellite, however, made 67 brightness measurements over the course of its three-year mission (Perryman et al. 1997) and failed to detect photometric variability. These results are consistent with the star’s low level of chromospheric and coronal activity (Delfosse et al. 1998).

We have acquired high-precision photometric observations of GJ 876 with the T12 0.8 m automatic photometric telescope (APT) at Fairborn Observatory to measure the level of photometric variability in the star, to derive its rotation period, and to assess the possibility of observing planetary transits in the GJ 876 system. The T12 APT is equipped with a two-channel precision photometer employing two EMI 9124QB bi-alkali photomultiplier tubes to make simultaneous measurements in the Strömgren b and y passbands. This telescope and its photometer are essentially identical to the T8 0.8 m APT and photometer described in Henry (1999). The APT measures the difference in brightness between a program star (P) and a nearby constant comparison star with a typical precision of 0.0015 mag for bright stars ($V < 8.0$). For GJ 876, we used HD 216018 ($V = 7.62$, $B - V = 0.354$) as our primary comparison star ($C1$) and HD 218639 ($V = 6.43$, $B - V = 0.010$) as a secondary comparison star ($C2$). We reduced our Strömgren b and y differential magnitudes with nightly extinction coefficients and transformed them to the Strömgren system with yearly mean transformation coefficients. Further information on the telescope, photometer, observing procedures, and data reduction techniques employed with the T12 APT can be found in Henry (1999) and Eaton, Henry, & Fekel (2003).

From June 2002 to June 2005, the T12 APT acquired 371 differential measurements of GJ 876 with respect to the $C1$ and $C2$ comparison stars. To increase the precision of these observations, we averaged our Strömgren b and y magnitudes into a single $(b+y)/2$ passband. The standard deviation of the $C1 - C2$ differential magnitudes from their mean is 0.0030 mag, slightly larger than the typical 0.0015 mag precision of the APT observations. However,

since the declination of GJ 876 is -14° , the APT observations are taken at a relatively high air mass, degrading the photometric precision somewhat. Periodogram analysis of the $C1 - C2$ differential magnitudes does not reveal any significant periodicity, indicating that both comparison stars are photometrically constant. However, the standard deviations of the GJ 876 differential magnitudes with respect to the two comparison stars, $P - C1$ and $P - C2$, are 0.0111 and 0.0110 mag, respectively, indicating definite variability in GJ 876. Our three sets of 371 $(b + y)/2$ differential magnitudes are given in Table 5.

The $P - C1$ differential magnitudes of GJ 876 are plotted in the top panel of Figure 15. Photometric variability of a few percent is clearly seen on a timescale of approximately 100 days; additional long-term variability is present as well. The light curve closely resembles those of typical late-type stars with low to intermediate levels of chromospheric activity (Henry, Fekel, & Hall 1995). Results of periodogram analysis of the data in the top panel are shown in the middle panel, revealing a best period of 96.7 days with an estimated uncertainty of approximately one day. We interpret this period to be the rotation period of the star, made evident by modulation in the visibility of photospheric starspots, which must cover at least a few percent of the stellar surface. The observations are replotted in the bottom panel, phased with the 96.7-day period and an arbitrary epoch, and clearly reveal the stellar rotation period.

There is little evidence from the photometric data for variability much shorter than the rotation period of the star. In particular, no photometric flares are apparent. On two nights when GJ 876 was monitored for several hours (JD 2453271 and JD 2453301), the star appears to be constant to better than 1%, consistent with our measurement precision over a large range of airmass. We conclude that photometric transits of the planetary companions could be observed in this star, if they occur, in spite of its intrinsic photometric variability.

8. Photometric Limits on Transits by GJ 876 “d”

The *a priori* probability that a planet on a circular orbit transits its parent star as seen from the line of sight to Earth is given by,

$$\mathcal{P}_{\text{transit}} = 0.0045 \left(\frac{1\text{AU}}{a} \right) \left(\frac{R_\star + R_{\text{pl}}}{R_\odot} \right) \quad (2)$$

where a is the semi-major axis of the orbit and R_\star and R_{pl} are the radii of the star and planet, respectively (Laughlin et al. 2005). We take $R_\star = 0.3 R_\odot$. For a given composition, planetary density increases with mass as higher pressures in the interior lead to greater self-compression. Léger et al. (2004) find that the mean density of a $6 M_\oplus$ planet with

composition similar to that of Earth would be $\sim 39\%$ greater than that of our planet. A $5.9 M_{\oplus}$ planet with such a density would have a radius of $1.619 R_{\oplus}$, or $0.0147 R_{\odot}$. Planets of comparable mass but containing significant quantities of astrophysical ices and/or light gases would be larger. The third companion’s orbital radius is ~ 0.021 AU. Thus, the *a priori* probability that the third companion transits GJ 876 is only $\sim 7\%$. The inclination of the orbit to the plane of the sky would have to be $\gtrsim 86^{\circ}$ ($\sim \arccos 0.07$) to guarantee periodic transits. Until recently, radial velocity measurements provided little constraint on the orbital inclinations of GJ 876’s planets (Laughlin et al. 2005), and they still are only able to exclude a trivial fraction of possible orientation angles for planet d (Section 5). Benedict et al. (2002) astrometrically estimated companion b’s inclination to the plane of the sky to be $84 \pm 6^{\circ}$. If we assume this range of possible values for the system and that all three planets are nearly coplanar, the probability of a transit by companion d rises to $\sim 25\%$. With a radius of $1.619 R_{\oplus}$, the transit depth is expected to be of order 0.22% , which is photometrically detectable by medium and large aperture telescopes. Additionally, the transit duration can be as long as $(\arcsin 0.07/\pi)P_d$, or slightly over an hour.

We used previous N-body fits to generate model radial velocities, which were then used to predict transit epochs for October, 2003. We examined the reflex radial velocity of the star due to just planet d; this motion is almost periodic, as perturbations of planet d by planets b and c are small. For a planet on a circular orbit, transit centers should coincide with times when the portion of the reflex velocity due to just the inner companion goes from positive (red shifted) to negative (blue shifted).

Since the probability that planet d transits the face of its star is relatively large, we obtained CCD photometry with the SITE#3 camera (2048x3150 $15 \mu\text{m}$ pixels) at the Henrietta Swope 1 m telescope at Las Campanas, in an attempt to detect such transits. We observed for 6 consecutive nights (UT dates 10 to 15 Oct 2003), with possible transits expected (based on the RV ephemeris and the 1.94-day orbital period) during the nights of 10, 12, and 14 Oct. We took all observations using a Harris V filter; integration times were typically 100 s to 120 s, depending upon seeing and sky transparency. With overheads, the observing cadence was about 245 s per image; on a typical night we obtained about 60 images, with a total of 355 usable images for the 6-night run. The nights of 10, 11, and 15 Oct were of photometric quality or nearly so; on 12, 13, and 14 Oct, each night began with an interval (roughly an hour long) of thin to moderate cirrus over the target field. Integration times were necessarily long in order to maintain a moderate duty cycle, and to accumulate enough total exposure time to reduce noise from atmospheric scintillation to acceptable levels. To avoid detector saturation for these relatively bright stars, we therefore defocused the images to a width of about 30 CCD pixels.

Each CCD integration contained the image of GJ 876, as well as those of 10 other stars that were bright enough to use as comparison objects. We computed the extinction-corrected relative flux (normalized to unity when averaged over the night of 10 Oct) of GJ 876 from the CCD images using proven techniques for bright-star CCD photometry, as described by, e.g., Gilliland & Brown (1992). We removed residual drifts with typical amplitudes of 0.002 (which we attribute to time-varying color-dependent extinction, combined with the extremely red color of GJ 876) from the time series of GJ 876 by subtracting a quadratic function of time (defined separately for each night). After this correction, the RMS variation of the relative flux for GJ 876 was in the range 0.001 to 0.0015 for each of the 6 nights.

We next searched for evidence of periodic transits by a small planet. We did this by folding the time series at each of a set of assumed periods, and then convolving the folded series with negative-going boxcar functions (rectangular window) with unit depth and with widths of 30, 45, and 60 minutes. We evaluated the convolution with the boxcar displaced from the start of the folded time series by lag times ranging from zero up to the assumed period, in steps of 0.005 day, or about 7 minutes. The convolution was normalized so that its value can be interpreted as the depth (in relative flux units) of a transit-like signal with the same width as the convolution boxcar function. Our transit detection statistic consisted of the normalized convolution, multiplied by the square root of the number of data points lying within the non-zero part of the boxcar at any given value of the lag. For most periods and phases, the number of included data points is about 15, so the detection statistic exceeds the transit depth by a factor of about 4. Since the expected duration of a transit by a short-period planet across an M4 dwarf is about 60 minutes, the range of boxcar widths covers both central and off-center transits, down to a duration for which the noise in the convolution becomes prohibitive. We tested periods between 1.8 and 2.0 days, on a dense period grid.

The solid curve in Figure 16 shows the logarithm of the histogram of the detection statistic, computed using all of the data. The largest transit-like events that occur in the data set have detection statistics of 0.0068, but the histogram is almost symmetrical about zero, so that there are very nearly as many positive-going boxcar events as negative-going ones. The value of the transit amplitude for the planet’s expected period and phase is 0.0005, assuming a 60-minute transit; this is about 1.3 standard deviations larger than zero. From the distribution of transit amplitudes, we estimate the probability that a true transit with amplitude 0.0015 is overlain by a negative-going noise spike with amplitude -0.001 (yielding an observed signal of 0.0005) is only about 2.4%. Thus, the observations contain no convincing evidence for planetary transits within the period range searched, and within the range of orbital phases probed by the data.

To refine our understanding of detectability, we added to the data synthetic transits with various depths and 60-minute duration; the phases were chosen so that transits occurred on each of the UT dates 10, 12, and 14 Oct. The dashed line in Figure 16 shows the resulting histogram of the detection statistic for synthetic transits with depth 0.0015. This histogram is plainly skewed toward positive values (negative-going transits), since real transits produce not only a few very large values of the detection statistic, but also many smaller ones (when the assumed period is not exactly correct, for instance). Examination of many realizations of synthetic transits suggests that the skewness shown in Figure 16 is near the limit of reliable detection. Adding synthetic transits with depths of 0.002, in contrast, always produces a histogram that is unmistakably skewed. Accordingly, we conclude that (within the period and phase limits already mentioned) there is no evidence for a transiting planet that obscures more than 0.002 of the star’s light, and it is highly improbable that there are transits with depth as great as 0.0015. Most likely, this is because the orbital inclination is such that transits do not occur. If transits are taking place, the maximum radius of the transiting body is approximately $\sqrt{0.002} R_\star = 9.4 \times 10^3$ km, or $1.47 R_\oplus$, assuming the radius of GJ 876 to be $0.3 R_\odot$. Assuming a maximum transit depth of 0.0015, the corresponding planetary radius is $1.28 R_\oplus$. Note that a larger planet can have a non-central transit.

Even though companion d was not transiting in 2003, it may transit in the future if the planets orbiting GJ 876 are on mutually inclined orbits. An analysis of the analogous case of possible transits by companion c is presented by Laughlin et al. (2005).

9. Discussion

The mass of GJ 876’s third companion is $\sim 7.5 M_\oplus$. Assuming this value of mass and a density of 8 g cm^{-3} to account for a bit more compression than that found for a $6 M_\oplus$ rocky planet by Léger et al. (2004), the planet’s radius is $1.73 R_\oplus$. The escape velocity from the surface would be slightly more than twice that of Earth, so that the planet may well have retained a substantial atmosphere, and may thus have a larger optical radius.

The proximity of GJ 876 d to its star implies that the timescale for tidal synchronization of its rotation to its orbital period is short for any reasonably assumed planetary properties. However, it is possible that atmospheric tides could maintain non-synchronous rotation, as they do on Venus (Dobrovolskis 1980). In analogy to models for Europa (Greenberg & Weidenschilling 1984), slightly non-synchronous rotation could result from an eccentric orbit forced by perturbations from the outer planets, especially if planet d lacks a substantial permanent asymmetry. Note in this regard that the topography of the planet’s surface, if it has one, is likely to be muted as a result of the high surface gravity (~ 2.5 times that of

Earth) and the expected malleability resulting from the planet’s large potential for retaining internal heat.

The mean effective temperature of a planet orbiting at $a = 0.021$ AU from a star with $L = 0.0124 L_{\odot}$ is $T_{\text{effective}} \sim 650(1 - A)^{1/4}$ K. Assuming that heat is uniformly distributed around the planet, as it is on Venus, and that the planet’s albedo does not exceed 0.8, its effective temperature should be in the range 430–650 K (157–377 C). Simulations by Joshi et al. (1997), suggest that synchronously rotating terrestrial planets with sufficiently massive atmospheres efficiently redistribute heat to their unlit hemispheres. For the opposite extreme of a synchronously rotating planet with no redistribution of stellar heat, the temperature at the subsolar point would be $\sqrt{2}$ higher at the substellar point, and varies as the 1/4th power of the cosine of the angle between the position of the star in the sky and the vertical (on the lit hemisphere), implying very cold values near the terminator, and the unlit hemisphere would be extremely cold.

We can conceive of numerous possible scenarios to explain the formation of GJ 876 d. If the planet is rocky, it could have formed in situ by accretion of small rocky planetesimals that spiraled inwards as a result of angular momentum loss through interactions with gas within the protoplanetary disk. At the other extreme, GJ 876 d may be the remnant core of a gas giant planet that migrated so close to its star that it lost (most of) its gaseous envelope to Roche lobe overflow (Trilling et al. 1998). Neptune/Uranus-like formation coupled with inwards migration models are also quite plausible, as well as various other combinations of accretion/migration scenarios. Additional observations of this and other small, close-in extrasolar planets will be required to narrow down phase space enough for us to have any confidence that any particular model is indeed the correct one.

The value of $\sqrt{\chi^2_{\nu}} = 1.065$ for our effective 14+1 parameter fit implies that the 3-planet coplanar inclined model provides an excellent fit to the data. Nonetheless, the fit is not perfect, and additional variations may be induced by stellar jitter and/or unmodelled small planets, as well as mutual inclinations of the three known planets. We note that the residuals to both the 90° and the 50° 1.94-day 3-planet fits to the data have modest power near 9 days (Figure 10); this period is also present in many of the residuals to artificial data sets used to test various aspects of the 3-planet fits. Somewhat larger peaks near 13 and 120 days are present in the residuals to the 50° fit. A small planet with an orbital period of around 13 days would be located so close to the massive and eccentric planet c that it would not be stable for long unless it occupied a protected dynamical niche. Even around 9.4 days, long-term stability is unlikely, especially if $i_c \lesssim 50^{\circ}$. The peak at 120 days probably represents an incomplete accounting of the radial velocity signature of the two large planets, but it could also represent a small outer planet on a resonant orbit. We note that Ji, Li,

& Liu (2002, private communication) performed simulations of the GJ 876 system with an additional planet with $a > 0.5$ AU. In agreement with Rivera & Lissauer (2001), all were found to be stable. More data are required to determine whether or not additional planets orbit GJ 876.

10. Summary

We have shown that the GJ 876 system likely has a low mass planet on a close-in orbit. Fitting a model that includes the previously identified jovian-mass companions to the radial velocity data obtained at the Keck telescope results in residuals that contain significant power at a periodicity of 1.9379 days. Including a third companion with this period in a self-consistent model results in a significant improvement in the quality of the fit. The third companion, which we refer to as GJ 876 d, is found to have a minimum mass of $5.89 \pm 0.54 M_{\oplus}$ and an orbital period of 1.93776 ± 0.00007 days. The corresponding semi-major axis is 0.021 AU, making it clearly the smallest a of any planet found in Doppler surveys. Note that this is ~ 10 stellar radii, roughly coincident with the number of stellar radii separating 51 Pegasi b from its host star. Planet d is also probably closer to its star in an absolute sense than are any of the planets found by transit. A significantly better fit to the data is obtained by assuming that the normal to the three planets' orbits is inclined to the line of sight by 50° than by assuming this inclination to be 90° . For this 50° fit, the actual mass of the inner planet is $7.53 \pm 0.70 M_{\oplus}$.

We have searched for transits, and find no evidence of them. The lack of observable transits means that we cannot place direct observational constraints on planet d's radius and composition. The requirement that the planet be contained within its Roche lobe implies that its density is at least 0.075 g cm^{-3} , not a very meaningful bound. Thus, while the newly discovered companion may well be a giant rocky body, a large gaseous component cannot be excluded. Continued study of GJ 876 will provide us with additional information on companion d, which may well be the most "Earth-like" planet yet discovered. See Table 4 for our best estimates of the masses and orbital parameters of all three planets now known to orbit GJ 876.

We thank Drs. Ron Gilliland, Mark Phillips, and Miguel Roth for informative advice and consultation during the observations performed at Las Campanas. We also are grateful for the contributed algorithms by Jason T. Wright, Chris McCarthy, and John Johnson. We thank Drs. Peter Bodenheimer, Eric Ford, Man Hoi Lee, and Sara Seager for useful discussions. We are also grateful to Sandy Keiser for maintaining the computers used for this work

at the Dept. of Terrestrial Magnetism at the Carnegie Institution of Washington. We thank an anonymous referee for a thorough report which helped improve the paper. The work of EJR and JJJ on this project was funded by NASA Solar Systems Origins grant 188-07-21-03 (to JJJ). The work of GL was funded by NASA Grant NNG-04G191G from the TPF Precursor Science Program. We acknowledge support from the Carnegie Institution of Washington and the NASA Astrobiology Institute through Cooperative Agreement NNA04CC09A for EJR's work on photometric studies. We acknowledge support by NSF grant AST-0307493 and AST-9988087 (to SSV), travel support from the Carnegie Institution of Washington (to RPB), NASA grant NAG5-8299 and NSF grant AST95-20443 (to GWM), and by Sun Microsystems. This research has made use of the Simbad database, operated at CDS, Strasbourg, France. We thank the NASA and UC Telescope Time Assignment committees for allocations of telescope time toward the planet search around M dwarfs. GWH acknowledges support from NASA grant NCC5-511 and NSF grant HRD-9706268. Finally, the authors wish to extend a special thanks to those of Hawaiian ancestry on whose sacred mountain of Mauna Kea we are very privileged to be guests. Without their generous hospitality, the Keck observations presented herein would not have been possible.

REFERENCES

- Benedict, G. F., et al. 2002, *ApJ*, 581, L115
- Butler, R. P., Marcy, G. W., Williams, E., McCarthy, C., Dosanjuh, P., & Vogt, S. S. 1996, *PASP*, 108, 500
- Butler, R. P., Vogt, S. S., Marcy, G. W., Fischer, D. A., Wright, J. T., Henry, G. W., Laughlin, G., & Lissauer, J. J. 2004, *ApJ*, 617, 580
- Chambers, J. E. 1999, *MNRAS*, 304, 793
- Delfosse, X., Forveille, T., Mayor, M., Perrier, C., Naef, D., & Queloz, D. 1998, *AA*, 338, L67
- Dobrovolskis, A. 1980, *Icarus*, 41, 18
- Eaton, J. A., Henry, G. W., & Fekel, F. C. 2003, in *The Future of Small Telescopes in the New Millennium, Volume II - The Telescopes We Use*, ed. T. D. Oswalt (Dordrecht: Kluwer), 189
- Ford, E. 2005, *AJ*, 129, 1717
- Gilliland, R. L. & Brown, T. M. 1992, *PASP*, 104, 582

- Goldreich, P. & Soter, S. 1966, *Icarus*, 5, 375
- Greenberg, R. & Weidenschilling, S. J. 1984, *Icarus*, 58, 186
- Henry, G. W. 1999, *PASP*, 111, 845
- Henry, G. W., Fekel, F. C., & Hall, D. S. 1995, *AJ*, 110, 2926
- Henry, T. J. & McCarthy, D. W. 1993, *AJ*, 106, 773
- Ji, J., Li, G., & Liu, L. 2002, *ApJ*, 572, 1041
- Joshi, M. M., Haberle, R. M., & Reynolds, R. T. 1997, *Icarus*, 129, 450
- Kazarovets, E. V. & Samus, N. N. 1997, *IBVS No.* 4471
- Konacki, M. & A. Wolszczan, A. 2003, *ApJ*, 591, L147
- Laughlin, G., Butler, R. P., Fischer, D. A., Marcy, G. W., Vogt, S. S., & Wolf, A. S. 2005, *ApJ*, 622, 1182
- Laughlin, G. & Chambers, J. E. 2001, *ApJ*, 551, L109
- Lee, M. H. & Peale, S. J. 2003, *ApJ*, 592, 1201
- Léger, A. 2004, *Icarus*, 169, 499
- Lissauer, J. J. & Rivera, E. 2001, *ApJ*, 554, 114
- Marcy, G. W. & Butler, R. P. 1992, *PASP*, 104, 270
- Marcy, G. W., Butler, R. P., Vogt, S. S., Fischer, D. A., & Lissauer, J. J. 1998, *ApJ*, 505, 147
- Marcy, G. W., Butler, R. P., Fischer, D., Vogt, S. S., Lissauer, J. J., & Rivera, E. J. 2001, *ApJ*, 556, 392
- Marcy, G. W., Butler, R. P., Fischer, D. A., Laughlin, G., Vogt, S. S., Henry, G. W., & Pourbaix, D. 2002, *ApJ*, 581, 1375
- Nauenberg, M. 2002, *ApJ*, 568, 369
- Perryman, M. A. C. et al. 1997, *AA*, 323, 49

- Press, W. H., Teukolsky, S. A., Vetterling, W. T., & Flannery, B. P. 1992, *Numerical Recipes: The Art of Scientific Computing* (2nd Edition; Cambridge, U.K.: Cambridge University Press)
- Rasio, F. A., Tout, C. A., Lubow, S. H., & Livio, M. 1996, *ApJ*, 470, 1187
- Rivera, E. J. & Lissauer, J. J. 2001, *ApJ*, 558, 392
- Trilling, D. E., Benz, W., Guillot, T., Lunine, J. I., Hubbard, W. B., & Burrows, A. 1998, *ApJ*, 500, 428
- Vogt et al. 1994, In *Proc. SPIE Instrumentation in Astronomy VIII*, David L. Crawford; Eric R. Craine; Eds., Volume 2198, p. 362
- Weis, E. W. 1994, *AJ*, 107, 1135
- Wolszczan, A. & Frail, D. 1992, *Nature*, 355, 145

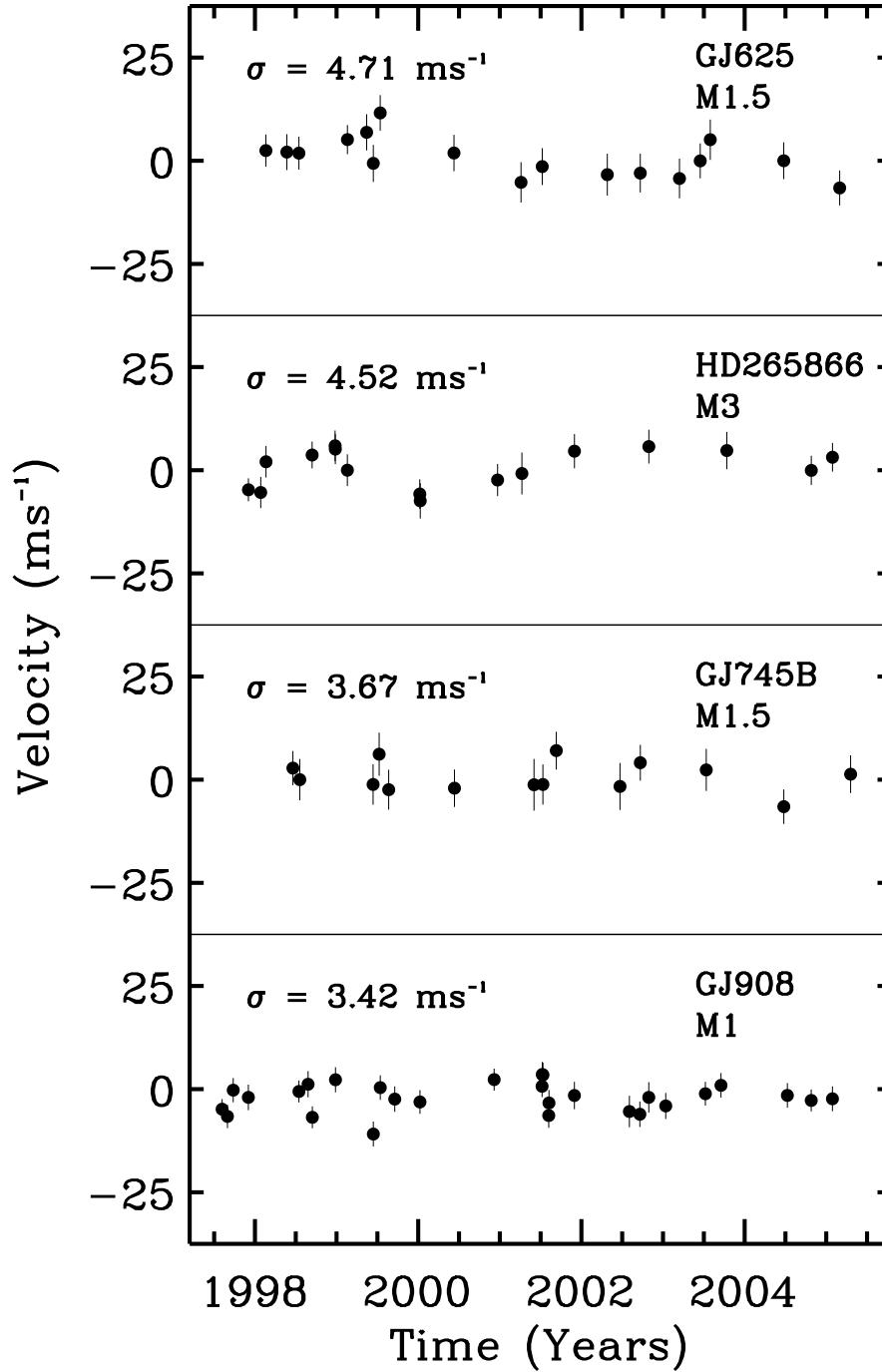


Fig. 1.— Radial velocity versus time for Keck M dwarfs spanning 7 years. The Keck-HIRES system achieves precision of 3–5 ms^{-1} for M dwarfs brighter than $V = 11$.

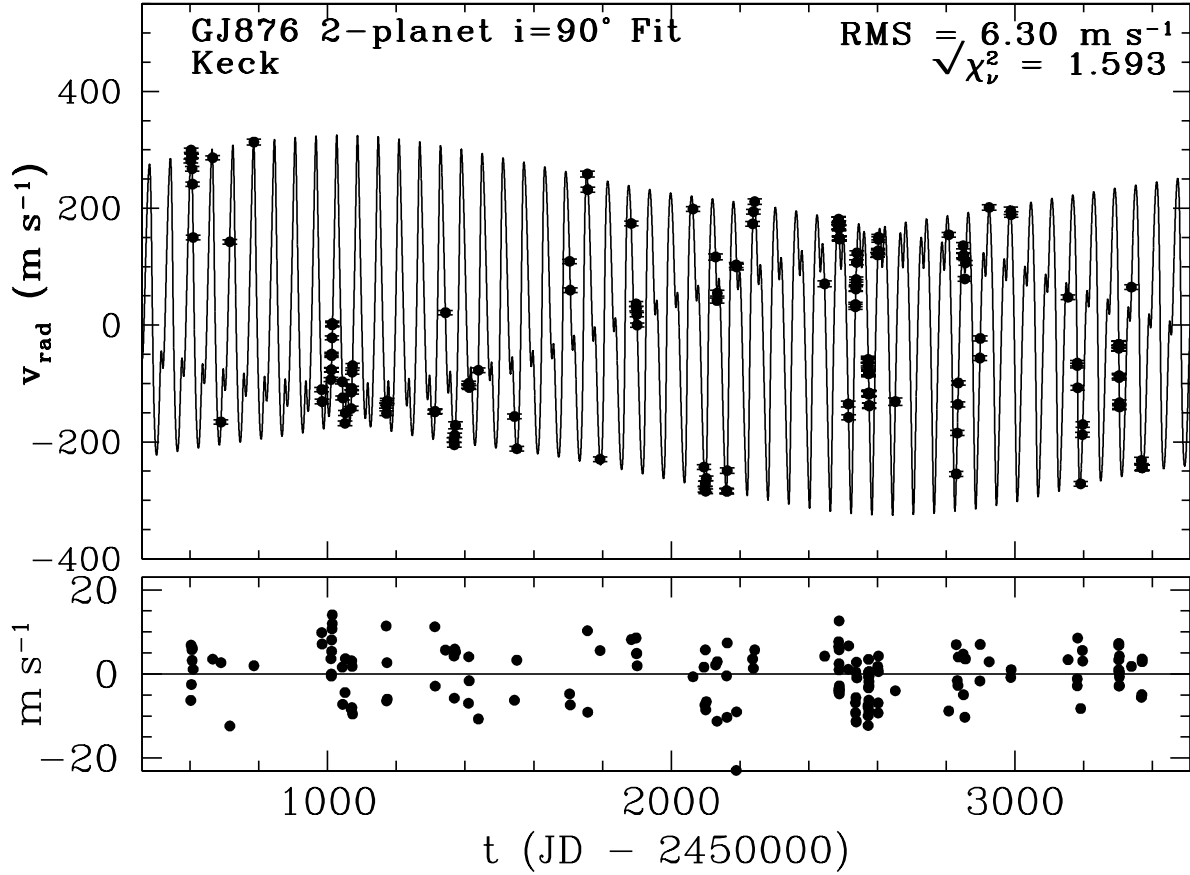


Fig. 2.— Top: Velocity versus time for GJ 876 with model radial velocity (solid line) generated from the nominal self-consistent, coplanar, $i = 90^\circ$, three-body (two-planet) fit to the observed radial velocities. The observed velocities (from Table 1) are shown as small solid points with vertical error bars corresponding to the instrumental uncertainties. Bottom: Residuals to the orbital fit.

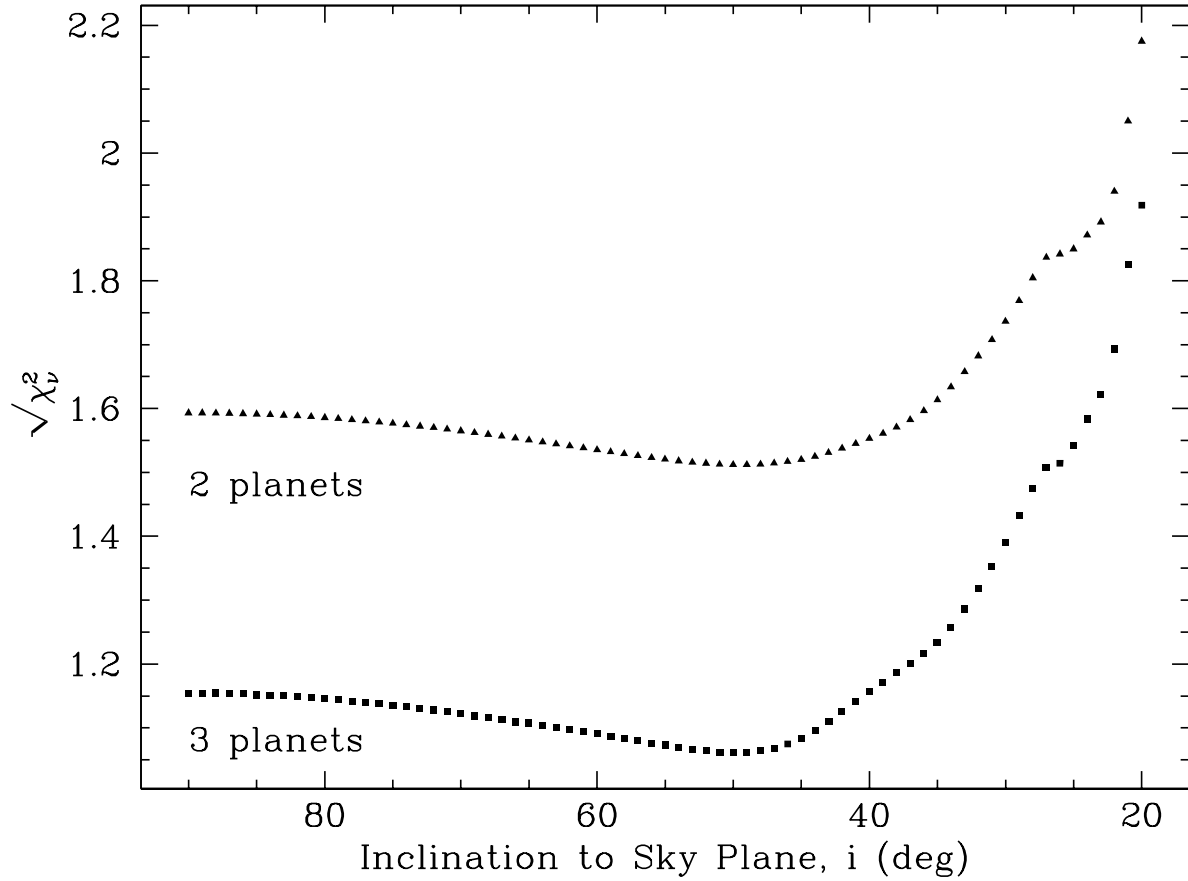


Fig. 3.— $\sqrt{\chi^2_\nu}$ values obtained from three-body (two-planet, triangles) and four-body (three-planet, squares) fits to the actual GJ 876 radial velocity data as a function of the inclination of the (assumed coplanar) system to the plane of the sky, i .

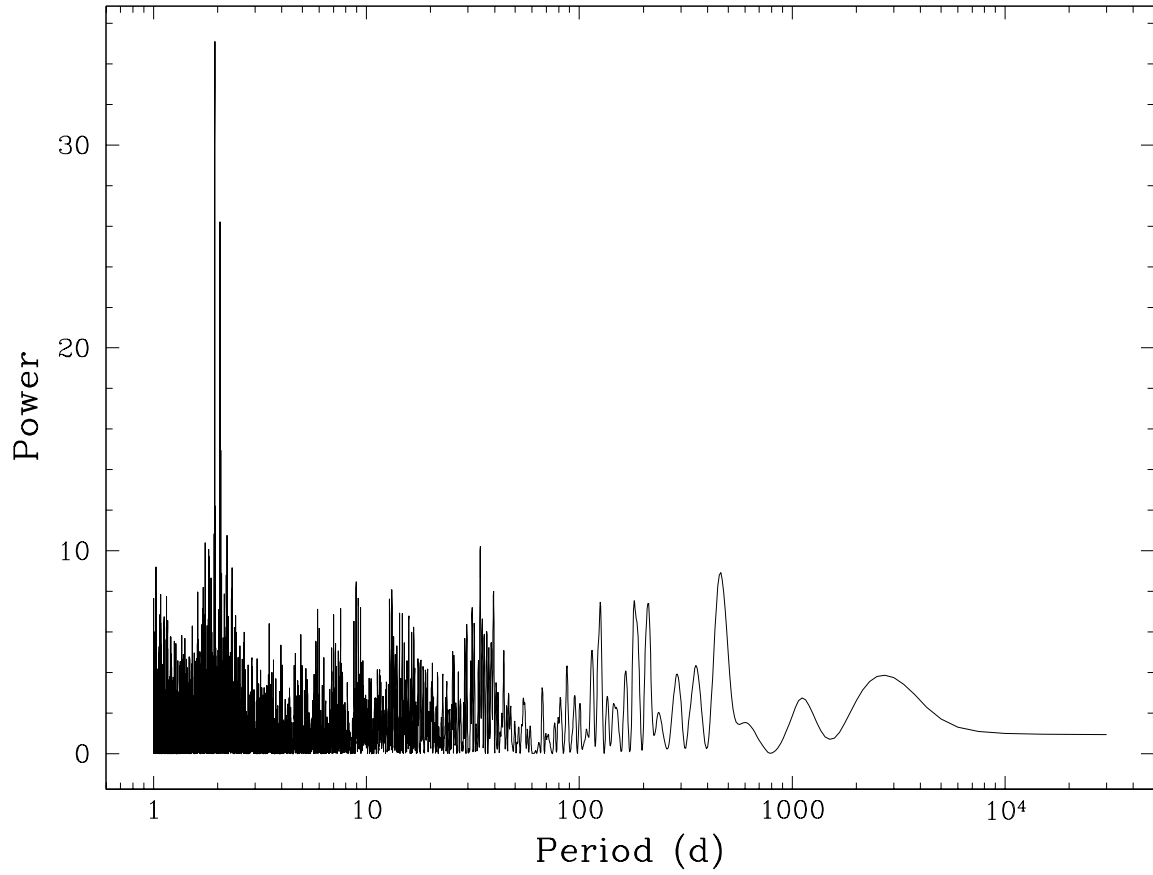


Fig. 4.— Periodogram of Residuals to the nominal two-planet, $i = 90^\circ$, coplanar fit, presented in Table 2 and Figure 2. Note the strong power at 1.938 and 2.055 days.

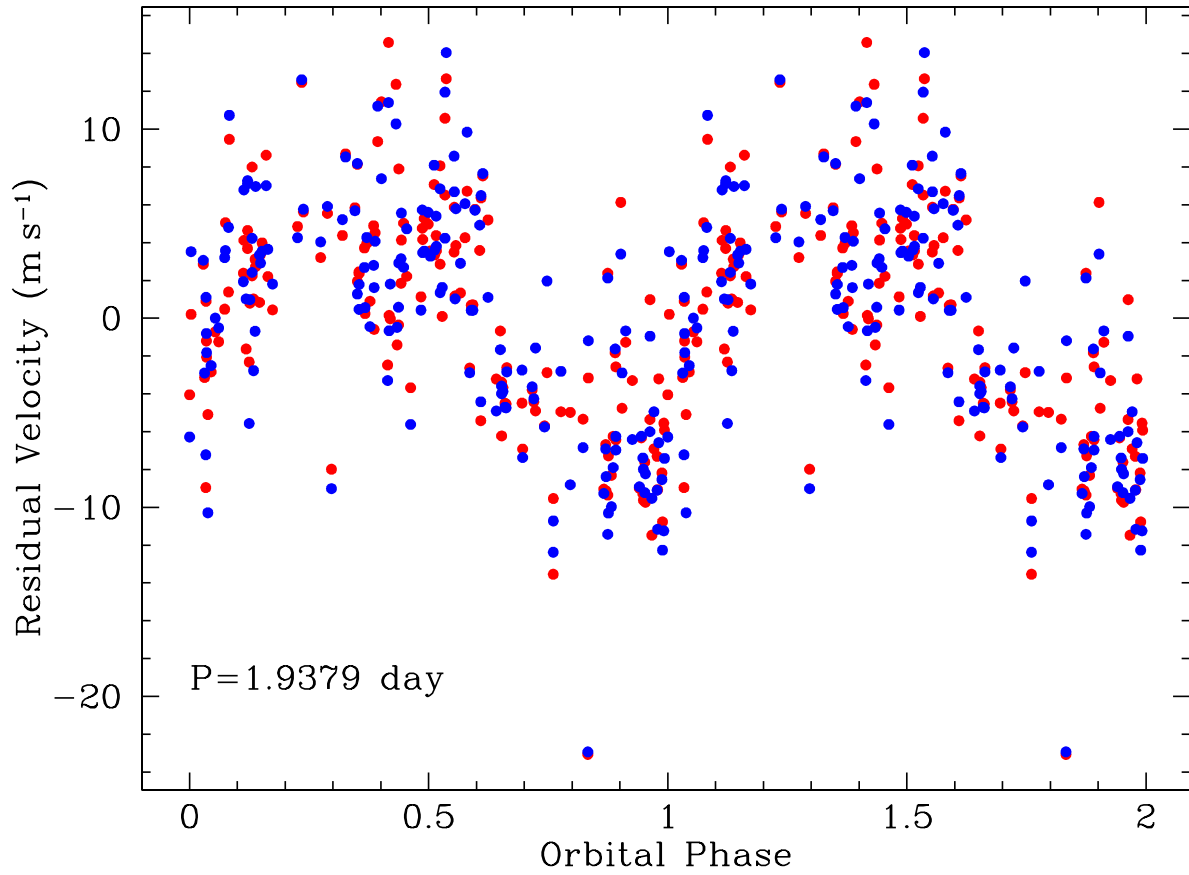


Fig. 5.— Blue: residuals to the nominal two-planet, $i = 90^\circ$, coplanar fit. Red: residuals to the two-planet, $i = 50^\circ$, coplanar fit. These residuals have been folded at the period of tallest peak shown in Figure 4, with the epoch of the first observation defining zero orbital phase. All points are plotted twice (as two cycles) to improve the visibility of the pattern.

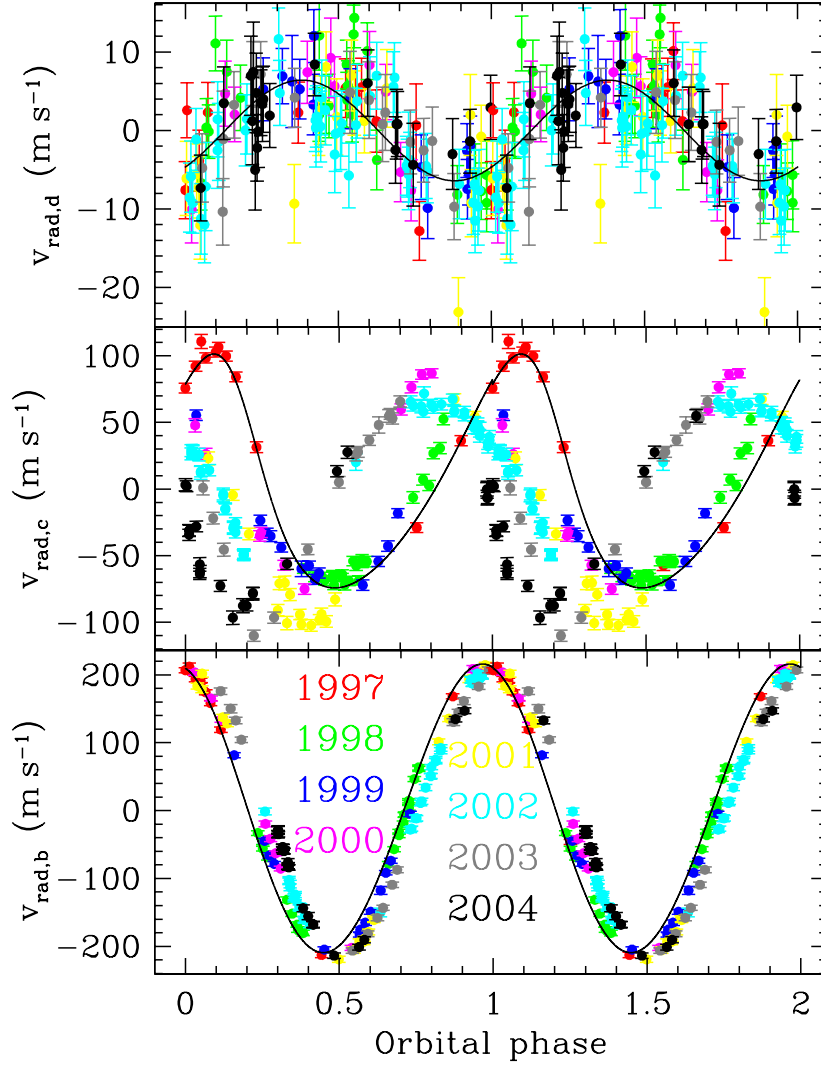


Fig. 6.— Triple-Newtonian orbital fit to the radial velocity observations for GJ 876. The observed and model velocities for each planet are shown separately by subtracting the effects of the other two planets. The panels show the velocities due to companions d (top), c (middle), and b (bottom). The curves show model velocities for the first orbital period beginning with the epoch of the first observation. The data were folded at the appropriate periodicity given by the fit in Table 3. Note the differences in scale in the three panels. The deviations shown for companions c and b clearly demonstrate that their orbital elements have been evolving over the timespan of the observations. The colored numbers in the bottom panel indicate which points correspond to which observing season. Note that the points taken in 1997 most closely follow the curves in the bottom two panels, as expected.

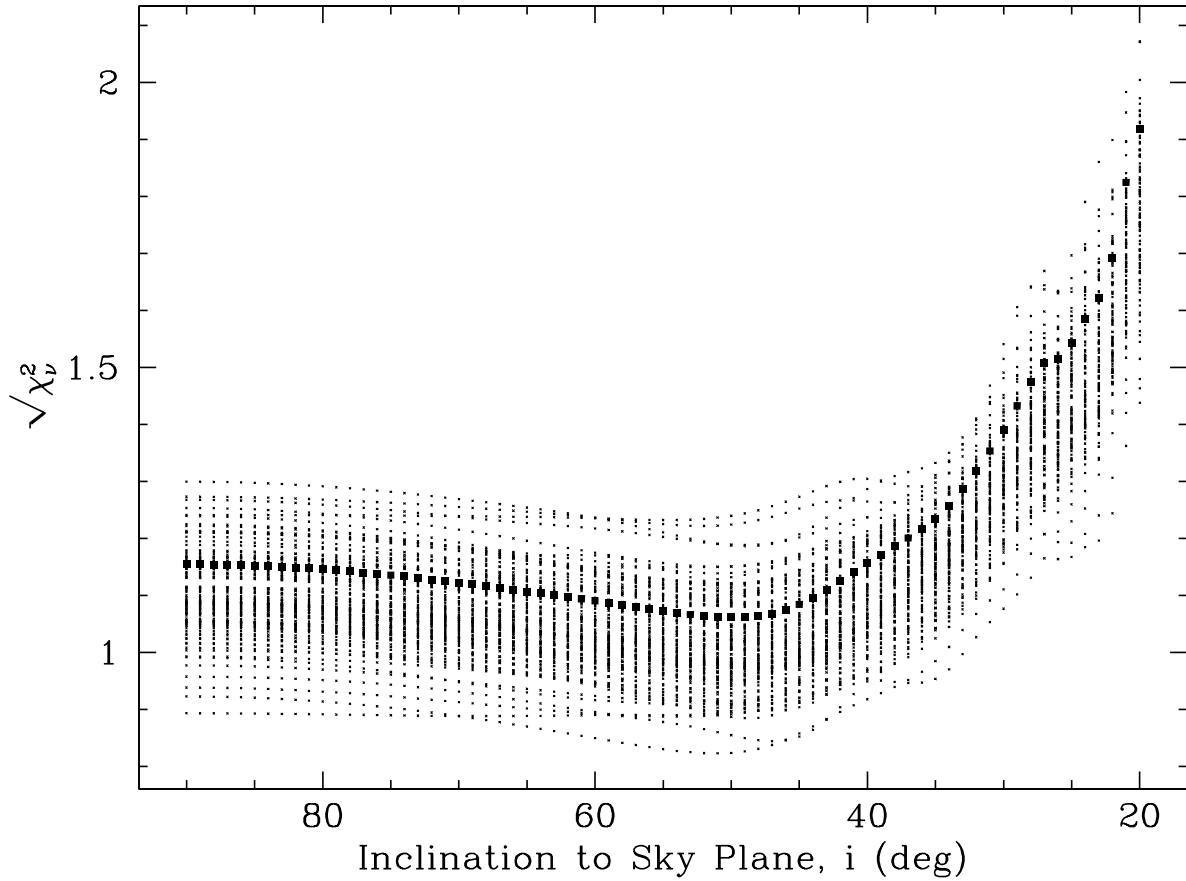


Fig. 7.— One hundred sets of results showing $\sqrt{\chi_v^2}$ versus the inclination to the plane of the sky, i , for 3-planet models to 100 generated radial velocity data sets (small points). The squares show the result of fitting the actual data. Note that most of the results for the generated velocity data sets have a minimum near $i = 50^\circ$, as for the result for the real velocity data set.

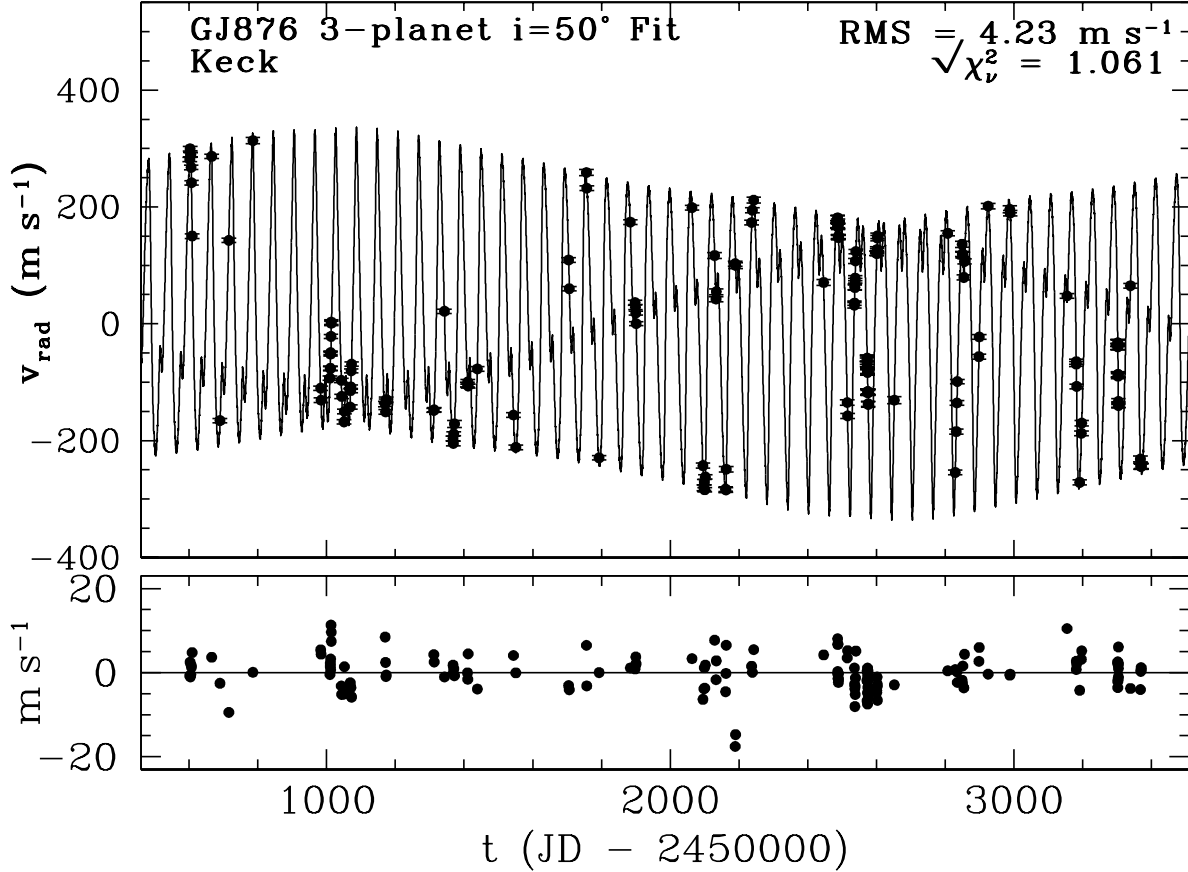


Fig. 8.— Top: Model radial velocity (solid line) generated from the self-consistent, coplanar, $i = 50^\circ$, four-body (three-planet) fit to the observed radial velocities for GJ 876. The observed velocities (from Table 1) are shown as small solid points with vertical error bars corresponding to the instrumental uncertainties. Bottom: Residuals to the orbital fit. Note that the $\sqrt{\chi^2_\nu}$ is 1.06, much lower than for the 2-planet model ($\sqrt{\chi^2_\nu} = 1.59$) and somewhat lower than the 3-planet model with $i = 90^\circ$.

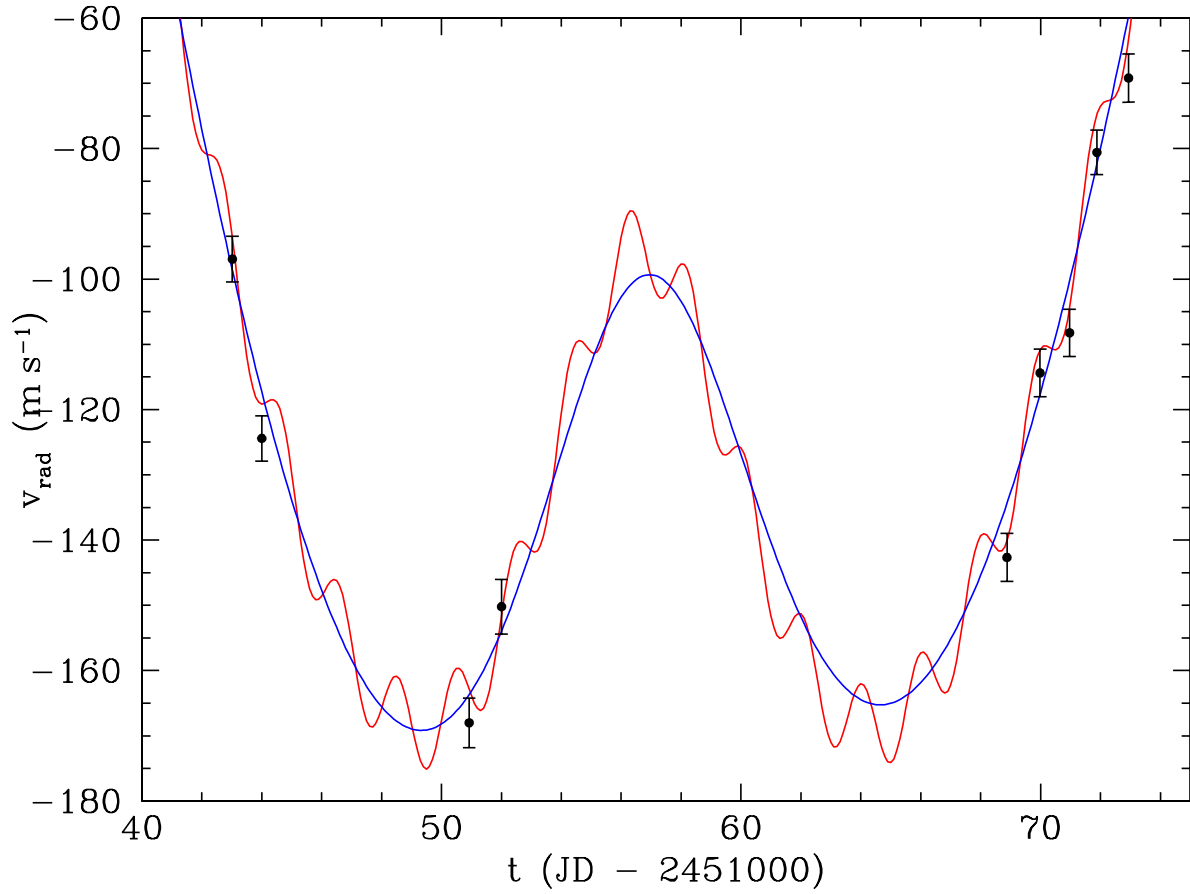


Fig. 9.— Zoom in near JD 2452060 on the model radial velocities from the two-planet $i = 90^\circ$ model shown in Figure 2 (blue curve) and the three-planet $i = 50^\circ$ model shown in Figure 8 (red curve) with the data overplotted.

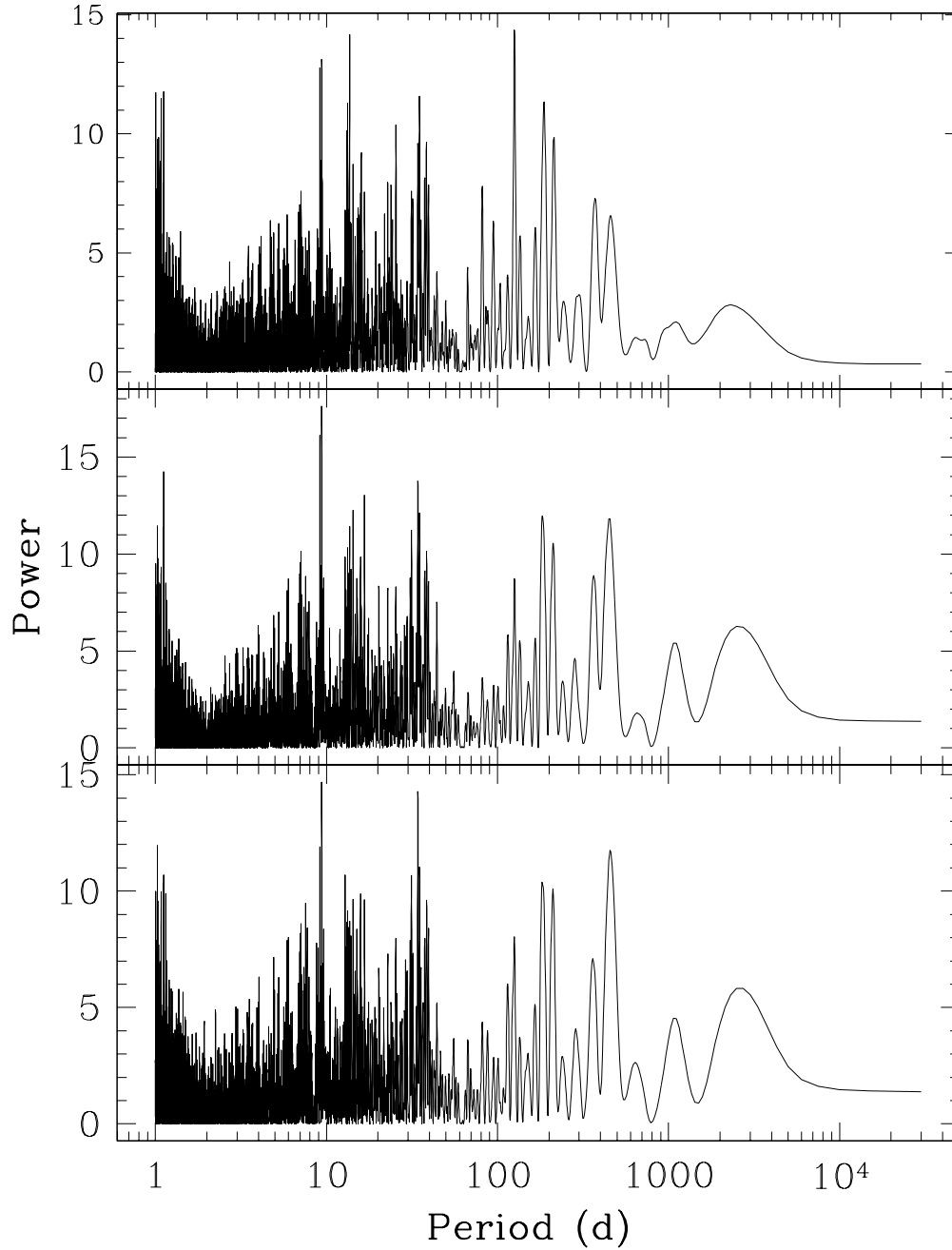


Fig. 10.— Top: Periodogram of residuals to the $i = 50^\circ$ 3-planet self-consistent fit (with $P_d = 1.9379$ days). Middle: Periodogram of Residuals to the nominal, $i = 90^\circ$, 3-planet, self-consistent fit with $P_d = 1.9379$ days. Bottom: Periodogram of Residuals to the nominal, $i = 90^\circ$, 3-planet, self-consistent fit with $P_d = 2.0548$ days.

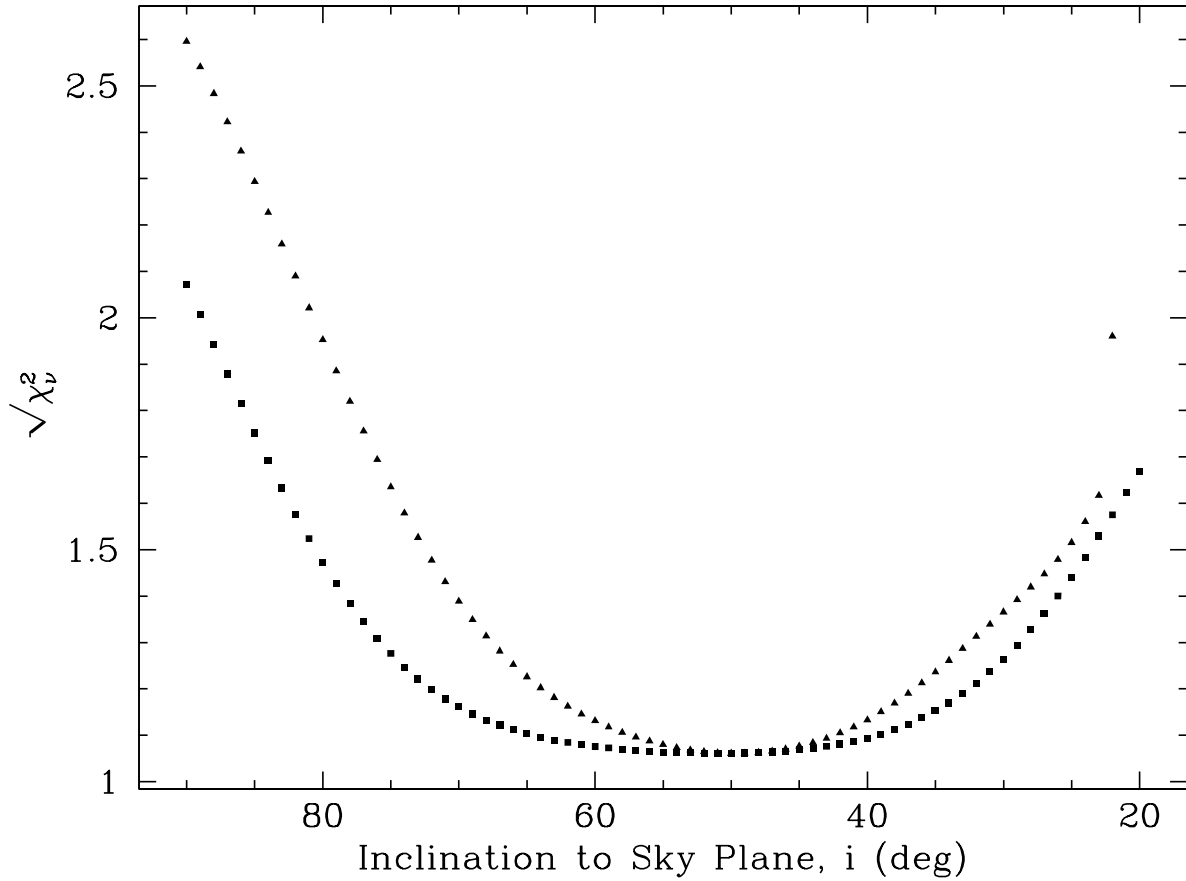


Fig. 11.— $\sqrt{\chi^2_v}$ versus the inclination to the plane of the sky for 3-planet configurations in the GJ 876 system in which the inclination of one of the outer planets is varied while the inclination of the remaining two planets is $i = 50^\circ$. Triangles show the effect of varying the inclination of planet b, while squares show the result of varying the inclination of companion c. All three nodes were aligned.

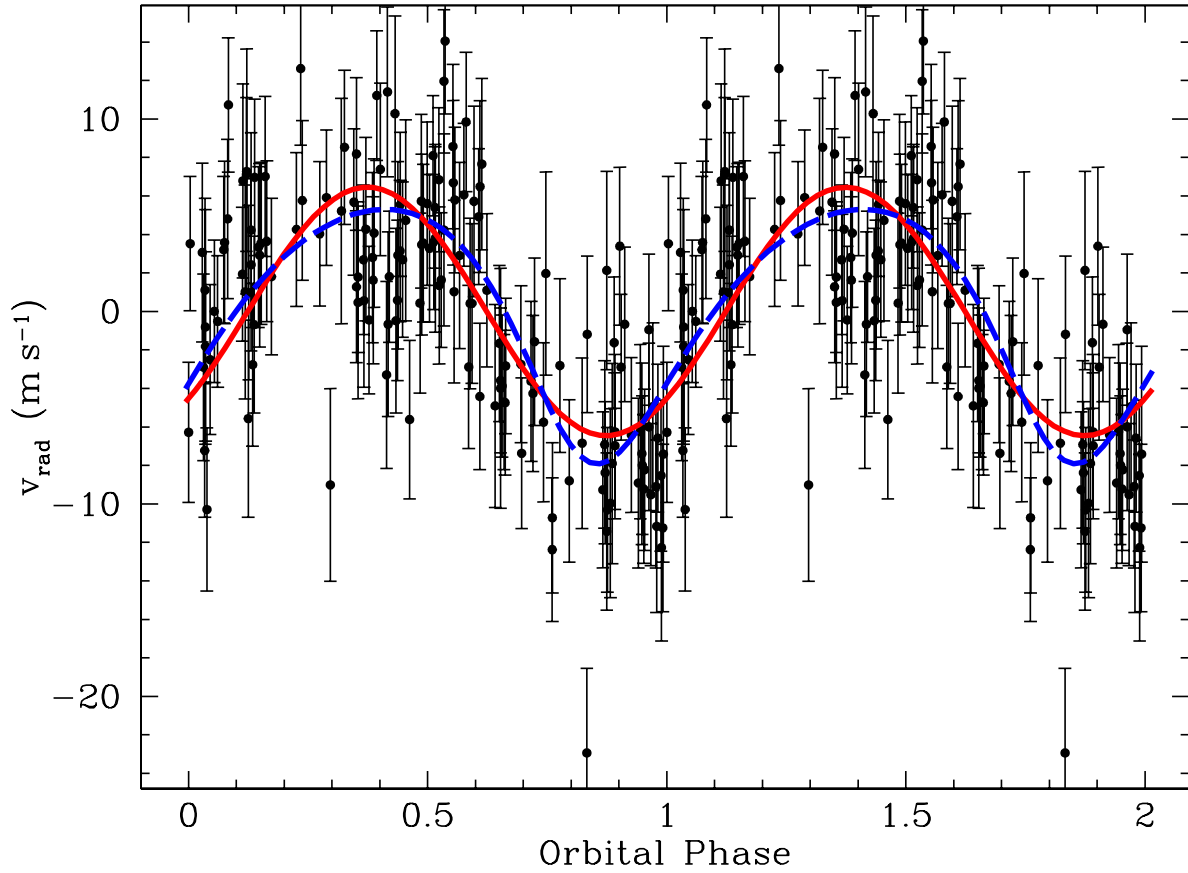


Fig. 12.— Model radial velocities generated from one-planet fits to the residuals of the $i = 90^\circ$ two-planet fit to the observed radial velocities for GJ 876. The solid red line is for a fit with $e_d = 0$, and the dashed blue line is for a fit with $e_d = 0.22$. The residual velocities are phased with a period of 1.9379 days and are shown as small solid points with vertical error bars corresponding to the instrumental uncertainties.

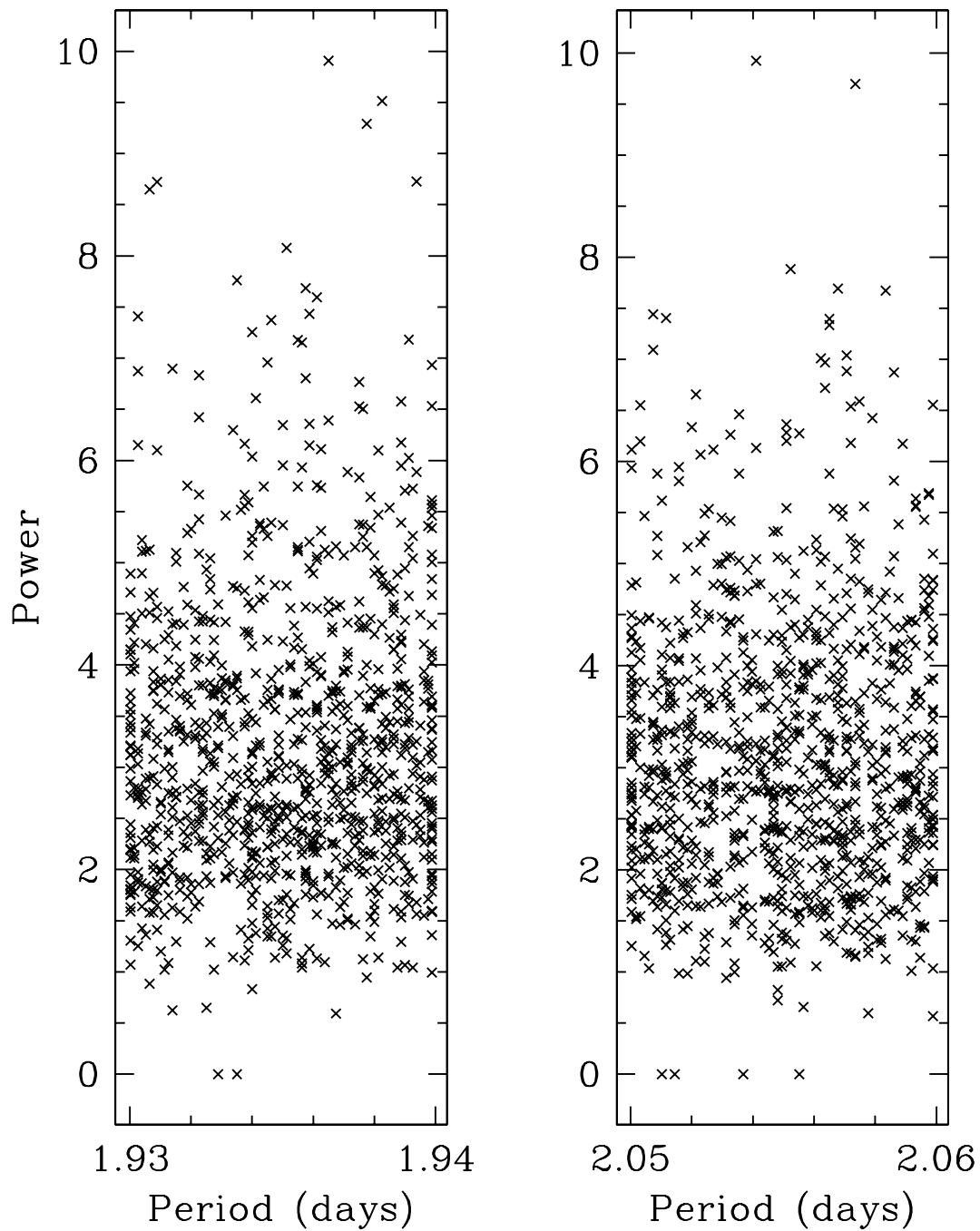


Fig. 13.— Maximum power at 1.94 days (left) and 2.05 days (right) in 1000 periodograms of residuals to two-planet fits to 1000 synthetic velocity data sets generated from a two-planet model.

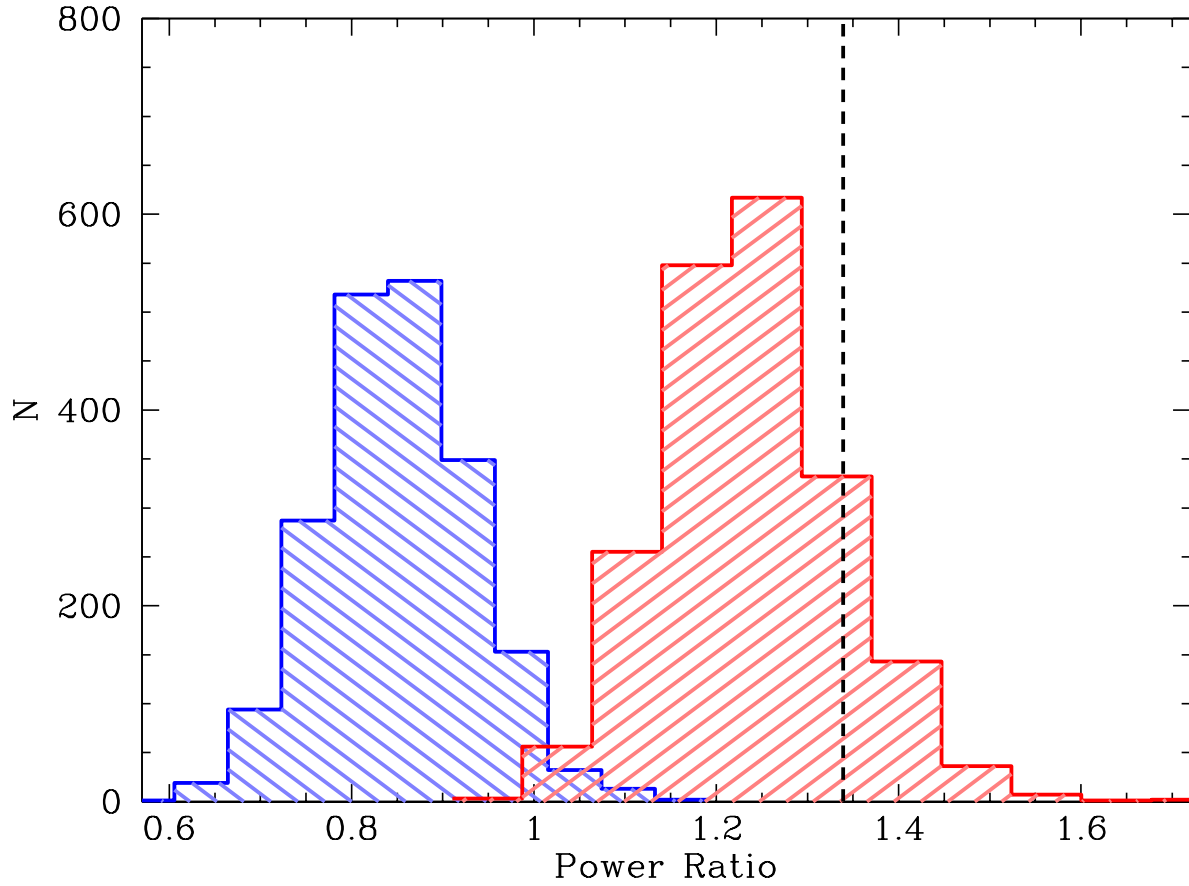


Fig. 14.— Histograms of the ratio of the power at 1.94 days to the power at 2.05 days for 4000 periodograms of residuals to two-planet fits to mock velocities generated from 3-planet models. Red shows the results when the third planet has a period of 1.94 days. Blue shows the results when the third planet has a period of 2.05 days. The dashed line at 1.3394 indicates the ratio observed in the periodogram of the residuals of the $i = 90^\circ$ two-planet fit to the actual data.

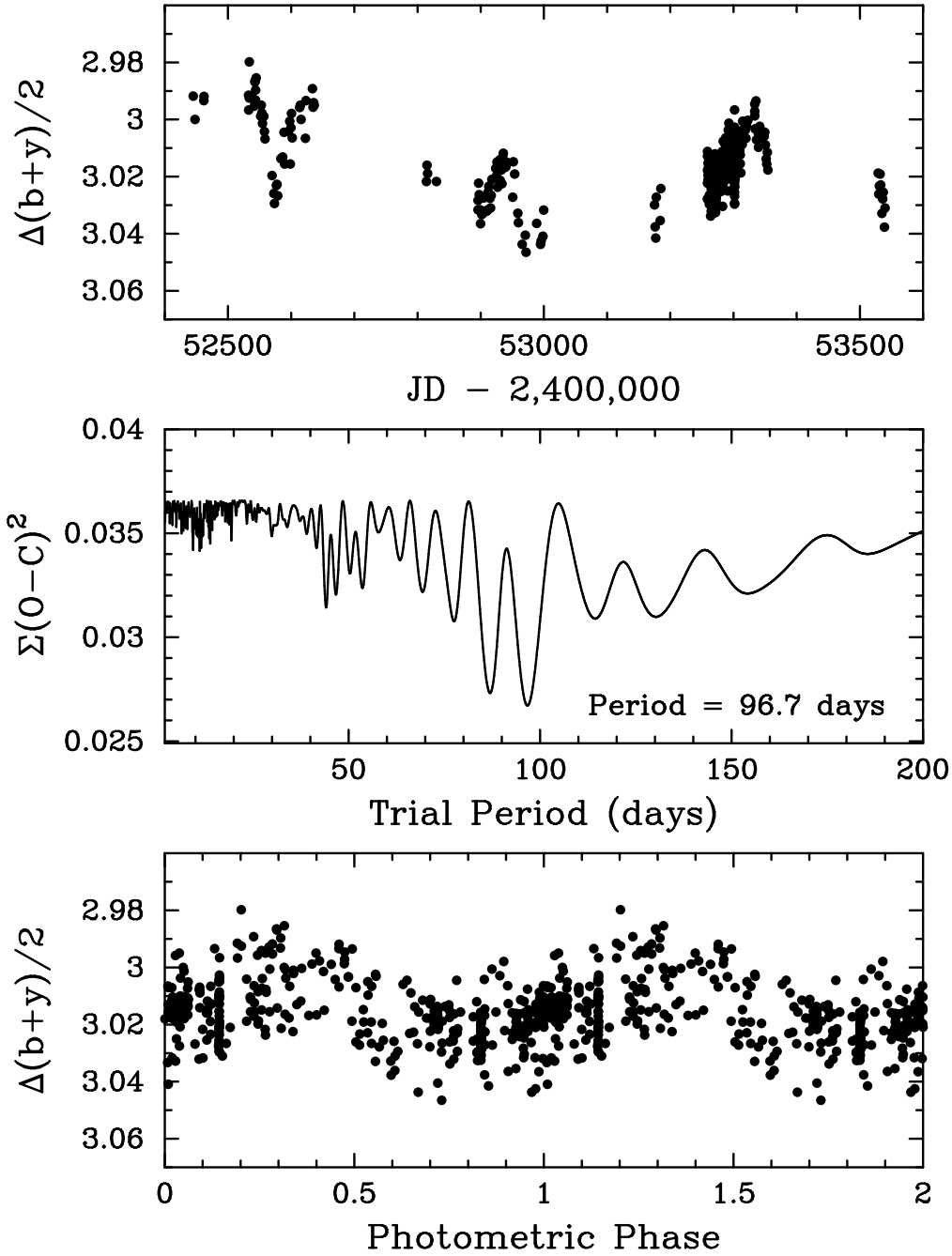


Fig. 15.— (*Top*): Photometric observations of GJ 876 with the T12 0.8 m APT demonstrate variability of a few percent on a timescale of approximately 100 days along with longer-term variability. (*Middle*): Periodogram analysis of the APT observations gives the star’s rotation period of 96.7 days. (*Bottom*): The photometric observations phased with the 96.7-day period reveal the effect of rotational modulation in the visibility of photospheric starspots on GJ 876.

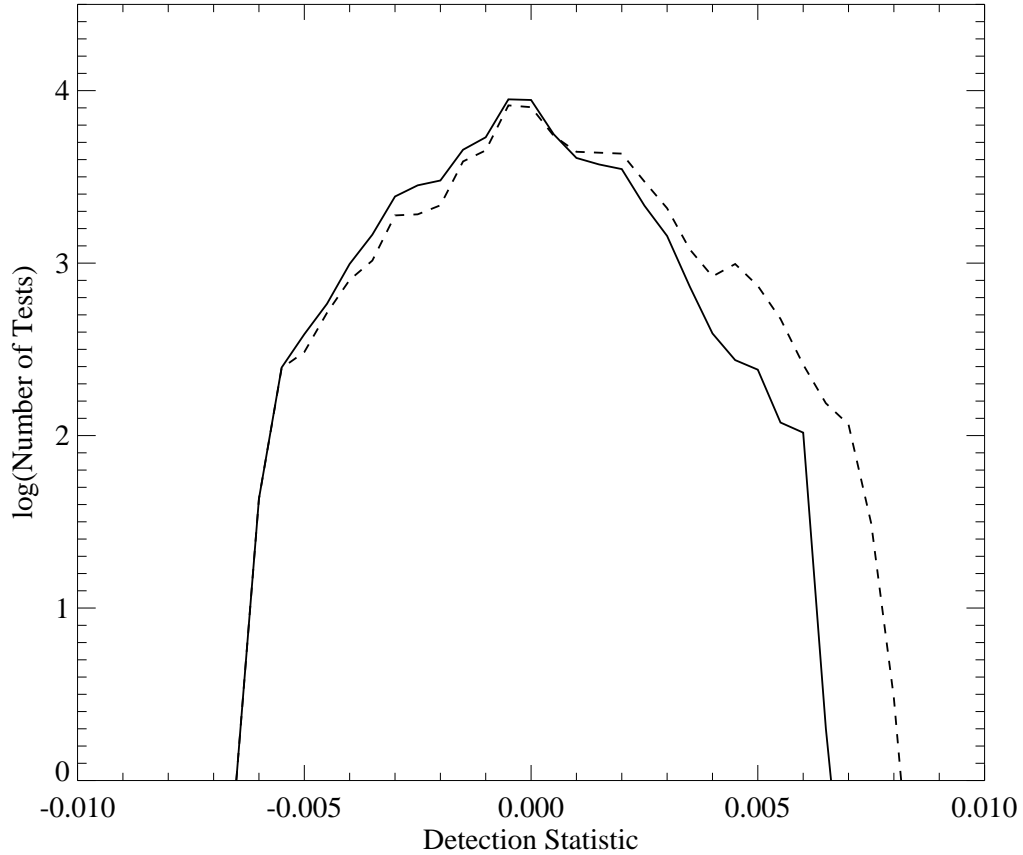


Fig. 16.— (Solid curve) Histogram of the logarithm, base 10, of the number of period/phase combinations tested as a function of their resulting transit detection statistics, for the full 6 nights of photometric data. See text for a definition of the transit detection statistic. Note that this curve is virtually symmetric about the value of 0, consistent with no transits being observed. (Dashed curve) Similar histogram for identical data to which artificial transits with relative flux depth of 0.0015 have been added, at a period of 1.900 days.

Table 1. Measured Velocities for GJ 876 (Keck)

JD (-2450000)	RV (m s^{-1})	Unc. (m s^{-1})
602.093	294.79	3.64
603.108	313.42	3.73
604.118	303.40	3.89
605.110	302.96	3.78
606.111	281.40	3.82
607.085	255.18	3.71
609.116	163.95	3.98
666.050	300.35	3.49
690.007	-151.95	3.88
715.965	156.45	3.73
785.704	327.19	5.28
983.046	-96.43	3.61
984.094	-117.02	4.00
1010.045	-79.21	3.51
1011.094	-62.54	3.70
1011.108	-62.78	3.42
1011.981	-35.71	3.12
1011.989	-38.23	3.15
1013.089	-7.85	3.49
1013.963	14.53	3.73
1013.968	16.75	3.80
1043.020	-83.07	3.51
1044.000	-110.55	3.47
1050.928	-154.13	3.81
1052.003	-136.35	4.18
1068.877	-128.79	3.68
1069.984	-100.52	3.67
1070.966	-94.38	3.60
1071.878	-66.73	3.41
1072.938	-55.33	3.69

Table 1—Continued

JD (-2450000)	RV (m s ⁻¹)	Unc. (m s ⁻¹)
1170.704	-123.56	4.41
1171.692	-137.08	4.02
1172.703	-119.17	4.04
1173.701	-115.95	4.35
1312.127	-134.51	3.37
1313.117	-133.52	3.79
1343.041	35.17	3.80
1368.001	-182.55	4.00
1369.002	-191.05	4.14
1370.060	-174.57	3.51
1372.059	-157.56	5.86
1409.987	-90.13	3.79
1410.949	-85.59	3.86
1411.922	-92.94	3.42
1438.802	-63.41	3.90
1543.702	-142.50	4.02
1550.702	-197.70	3.84
1704.103	122.99	3.76
1706.108	73.75	3.91
1755.980	272.62	5.08
1757.038	245.87	4.24
1792.822	-215.71	3.74
1883.725	187.77	3.96
1897.682	50.01	4.27
1898.706	42.34	4.14
1899.724	32.04	3.53
1900.704	13.98	3.47
2063.099	212.65	4.01
2095.024	-228.99	4.35
2098.051	-266.92	4.71

Table 1—Continued

JD (-2450000)	RV (m s ⁻¹)	Unc. (m s ⁻¹)
2099.095	-257.23	4.51
2100.066	-270.35	3.92
2101.991	-248.41	3.84
2128.915	130.58	5.15
2133.018	55.95	4.35
2133.882	68.55	4.86
2160.896	-269.15	3.84
2161.862	-270.68	4.28
2162.880	-235.10	4.49
2188.909	116.79	4.39
2189.808	113.52	5.00
2236.694	187.17	4.10
2238.696	208.12	4.08
2242.713	225.32	4.95
2446.071	84.52	4.99
2486.913	194.04	4.46
2486.920	195.16	4.46
2487.120	182.36	4.16
2487.127	181.67	4.06
2487.914	179.58	4.53
2487.923	180.93	4.48
2488.124	188.92	3.98
2488.131	181.99	4.15
2488.934	162.66	3.75
2488.940	162.29	3.69
2488.948	161.35	3.50
2488.955	163.13	3.52
2514.867	-121.06	4.78
2515.873	-143.91	4.27
2535.774	45.38	4.43

Table 1—Continued

JD (-2450000)	RV (m s ⁻¹)	Unc. (m s ⁻¹)
2536.024	49.11	3.87
2536.804	77.18	5.01
2537.013	75.82	4.12
2537.812	87.35	4.09
2538.014	91.81	4.48
2538.801	121.30	4.42
2539.921	137.37	3.92
2572.709	-46.62	4.91
2572.716	-44.75	5.20
2572.916	-54.73	4.85
2572.924	-50.10	5.60
2573.740	-69.21	4.86
2573.746	-66.75	4.80
2573.875	-69.37	4.68
2573.882	-66.53	4.70
2574.760	-104.45	4.41
2574.768	-102.01	4.53
2574.936	-103.60	4.85
2574.944	-102.76	4.91
2575.716	-124.28	4.80
2575.722	-123.40	4.16
2600.748	134.05	3.95
2600.755	134.67	3.92
2601.747	138.56	4.05
2601.754	141.02	4.35
2602.717	160.52	4.50
2602.724	164.31	4.77
2651.718	-116.96	6.23
2807.028	168.61	4.21
2829.008	-240.74	4.06

Table 1—Continued

JD (-2450000)	RV (m s ⁻¹)	Unc. (m s ⁻¹)
2832.080	-170.81	4.35
2833.963	-121.76	4.07
2835.085	-85.07	3.75
2848.999	149.86	5.22
2850.001	133.34	4.35
2851.057	131.25	4.89
2854.007	93.08	4.24
2856.016	120.42	4.22
2897.826	-42.50	4.05
2898.815	-8.85	4.16
2924.795	215.18	4.84
2987.716	209.59	6.10
2988.724	203.06	4.75
3154.117	61.47	4.10
3181.005	-51.18	4.51
3181.116	-55.10	4.07
3182.070	-93.33	4.00
3191.037	-257.70	4.19
3195.970	-173.67	4.25
3196.997	-156.17	4.64
3301.808	-18.93	5.04
3301.817	-25.17	5.55
3301.823	-19.23	6.37
3301.871	-25.66	4.18
3302.723	-75.85	4.24
3302.729	-72.85	4.43
3302.736	-73.20	4.15
3303.779	-119.03	5.06
3303.785	-126.29	4.23
3303.791	-124.47	4.60

Table 1—Continued

JD (-2450000)	RV (m s ⁻¹)	Unc. (m s ⁻¹)
3338.744	78.91	4.07
3367.718	-217.67	5.12
3368.719	-230.07	5.27
3369.702	-230.32	4.76
3369.708	-229.73	4.21

Table 2. Two-Planet $i = 90^\circ$ Parameters

Parameter	Planet c	Planet b
m^a	$0.617 \pm 0.007 M_{\text{Jup}}$	$1.929 \pm 0.009 M_{\text{Jup}}$
P (days)	30.344 ± 0.018	60.935 ± 0.017
K (m s ⁻¹)	88.12 ± 0.94	212.04 ± 1.03
a^a (AU)	0.13031 ± 0.00005	0.20781 ± 0.00004
e	0.2232 ± 0.0018	0.0251 ± 0.0035
ω (°)	198.3 ± 1.4	176.8 ± 9.2
M (°)	308.8 ± 1.9	174.3 ± 9.2
transit epoch	JD 2452517.604 \pm 0.067	

^aQuoted uncertainties in planetary masses and semi-major axes *do not* incorporate the uncertainty in the mass of the star

Table 3. Three-Planet $i = 90^\circ$ Parameters

Parameter	Planet d	Planet c	Planet b
m^a	$5.89 \pm 0.54 M_\oplus$	$0.619 \pm 0.005 M_{\text{Jup}}$	$1.935 \pm 0.007 M_{\text{Jup}}$
P (d)	1.93776 ± 0.00007	30.340 ± 0.013	60.940 ± 0.013
K (m s^{-1})	6.46 ± 0.59	88.36 ± 0.72	212.60 ± 0.76
a^a (AU)	0.0208067 ± 0.0000005	0.13030 ± 0.00004	0.20783 ± 0.00003
e	0 (fixed)	0.2243 ± 0.0013	0.0249 ± 0.0026
ω ($^\circ$)	0 (fixed)	198.3 ± 0.9	175.7 ± 6.0
M ($^\circ$)	309.5 ± 5.1	308.5 ± 1.4	175.5 ± 6.0
transit epoch	JD 2452490.756 \pm 0.027	JD 2452517.633 \pm 0.051	

^aQuoted uncertainties in planetary masses and semi-major axes *do not* incorporate the uncertainty in the mass of the star

Table 4. Three-Planet $i = 50^\circ$ Parameters

Parameter	Planet d	Planet c	Planet b
m^a	$7.53 \pm 0.70 M_\oplus$	$0.790 \pm 0.006 M_{\text{Jup}}$	$2.530 \pm 0.008 M_{\text{Jup}}$
P (d)	1.93774 ± 0.00006	30.455 ± 0.019	60.830 ± 0.019
K (m s^{-1})	6.32 ± 0.59	87.14 ± 0.67	212.81 ± 0.66
a^a (AU)	0.0208067 ± 0.0000004	0.13065 ± 0.00005	0.20774 ± 0.00004
e	0 (fixed)	0.2632 ± 0.0013	0.0338 ± 0.0025
ω ($^\circ$)	0 (fixed)	197.4 ± 0.9	185.5 ± 4.3
M ($^\circ$)	311.8 ± 4.6	311.6 ± 1.3	165.6 ± 4.2

^aQuoted uncertainties in planetary masses and semi-major axes *do not* incorporate the uncertainty in the mass of the star

Table 5. Photometric Observations of GJ 876

Hel. Julian Date (HJD – 2,400,000)	$P - C1$ (mag)	$P - C2$ (mag)	$C1 - C2$ (mag)
52444.9553	2.9918	4.2587	1.2668
52447.9492	3.0000	4.2730	1.2730
52461.9151	2.9934	4.2622	1.2689
52461.9541	2.9919	4.2609	1.2690
52532.7211	2.9915	4.2610	1.2694

Note. — Table 5 is presented in its entirety in the electronic edition of the *Astrophysical Journal*. A portion is shown here for guidance regarding its form and content.